Wear Behavior of Aluminum Alloys Made with Selective Laser Melting (SLM) Additive Manufacturing

by

Nicole Rae Christy

Bachelor of Science, Carlow University, 2010

Submitted to the Graduate Faculty of

Swanson School of Engineering in partial fulfillment

of the requirements for the degree of

Master of Science in Materials Science and Engineering

University of Pittsburgh

2019

UNIVERSITY OF PITTSBURGH

SWANSON SCHOOL OF ENGINEERING

This thesis was presented

by

Nicole Rae Christy

It was defended on

March 29, 2019

and approved by

Markus Chmielus, Ph.D., Assistant Professor
Mechanical Engineering and Materials Science

Wei Xiong, Ph.D., Assistant Professor
Mechanical Engineering and Materials Science

Thesis Advisor: Tevis Jacobs, Ph.D., Assistant Professor
Mechanical Engineering and Materials Science

Wear Behavior of Aluminum Alloys Made with Selective Laser Melting (SLM) Additive Manufacturing

Nicole Rae Christy, M.S.

University of Pittsburgh, 2019

The selective laser melting (SLM) additive manufacturing process produces material properties that differ from conventionally made parts. These properties such as mechanical behavior and tribological performance may benefit certain applications. This research investigates the wear resistance of SLM additive manufactured parts, motivated by the engine piston application, where high temperatures and harsh conditions lead to sliding wear and material degradation. Hypothesized is that SLM additive manufacturing can improve the mechanical properties and tribological performance over conventional alloys by tailoring the microstructure through modifications in energy density. Standard coupons of AlSi10Mg were produced with different build parameters on the contour face and these were compared to conventionally made aluminum alloys commonly used in the engine piston application. All the samples were analyzed for composition, microstructure, mechanical behavior, and wear performance. The results have shown that the changes made to increase energy density affect the microstructure, melt pools, and the wear performance of the AM SLM samples. The highest energy density AM SLM sample has differences in microstructure, melt pools, and an increased wear performance than the lower energy density AM SLM samples. The implications of this research are to better understand how SLM build parameters affect the mechanical and tribological performance of aluminum alloys, and how this can be leveraged to optimize performance beyond that of conventionally manufactured parts.

Table of Contents

List of Tables

List of Figures

1.0 Introduction

Additive manufacturing technology dates to the mid-1980s with the first commercial machine being an SLA-1 from 3D Systems. This technology allows the manufacturing of components into complex structural shapes that are difficult or impossible to produce by conventional processes like forging and casting. By using an additive manufactured part there is less material removal and less part-specific tooling compared to conventional parts. (Bourell, 2017)

There are several methods for additively manufacturing parts: Laser Beam Melting (LBM), Direct Metal Laser Sintering (DMLS), LaserCUSING, Laser Metal Fusion (LMF), Electron Beam Melting (EBM), and Laser Metal Deposition (LMD). In this study the method used to build additively manufactured aluminum parts is called Selective Laser Melting (SLM), a subset of Laser Beam Melting. (Herzog, 2016)

Selective laser melting applies a uniform thickness layer of metal alloy or aluminum alloy powder over the build area, then a laser source moves across the powder bed to melt powder particles to form a solid layer of the metal part. The laser moves according to a computer aided design (CAD) template to build the part layer by layer. This creates a part with the geometry specified by the CAD template.

The instrument includes operational settings (i.e. build parameters), such as laser power, laser velocity, hatch spacing, etc., programmed into the instrument that impact part characteristics such as surface and bulk mechanical properties, microstructure, porosity, and surface finishes. Build parameters vary based on the local region and orientation of the part as it is being built. (Herzog, 2016)

Powder characteristics also affect the part characteristics. Material characteristics of the powder include alloy type, chemical composition, and printability. Geometric powder characteristics include powder shape, particle size distribution, and morphology.

Both the build parameters and the powder characteristics interact affecting the finished part. Surface finish and final mechanical and physical properties illustrates the interactions. Some of those interactions include energy absorption (temperature) during building, the deposit geometry, solidification of the powder, resulting microstructure, and melt pool. (Bourell, 2017)

Engine pistons are the target application addressed in the study. The sliding conditions that they experience is a sliding motion back and forth against the cylinder side walls. This sliding motion is periodic and dictated by the engine combustion environment. Pistons are exposed to extreme temperature and pressure conditions to obtain maximum engine efficiency. This makes high temperature and high strength materials desirable for this type of application. (Piston and Piston Rings, 1996)

There are two different types of piston design objectives that could be targeted to understand mechanical properties, physical properties, and wear mechanics. They are high durability and high performance. High durability pistons are generally cast products that are not made with strong materials and are less expensive to produce. Engines that use high durability pistons generally do not have a customer willing to pay for higher performance pistons and engines. High performance pistons have a different target customer base which includes high end vehicles and high-performance vehicles. High-performance pistons are forged, made with stronger materials, and are more expensive to produce. Some improvements that the high-performance pistons could benefit from are extended exposures at high temperatures, lighter weight, and high material strength which allows for thinner pistons which in turn would maximize fuel economy and lessen cyclic mechanical loadings.

Additive manufacturing can produce hard-to-manufacture components in complex structural shapes that are difficult or time-consuming to fabricate by conventional means. Additively manufactured pistons might take longer to make than a forging, but that forging would have additional machining steps that are both costly and time-consuming. Thus, the true cost of these respective processes must consider any additional steps not studied here. That said, the cost of making an additively manufactured piston is higher than a conventionally made piston (forged or cast) which is why there must also be a willingness to pay from the high-performance customer base for this type of product.

2.0 Background Information on Selective Laser Melting and the Aluminum Alloys Under Investigation

Additive manufacturing has become an established option for creating complex and hard-to-build parts. Gaining an understanding of how build parameters that affect energy density have an impact on the resulting microstructure and material properties, mechanical and physical, will help grow the technology. There are many different methods to additively manufacture parts and this paper will focus on selective laser melting. In this chapter, a review of AM SLM, the target application, and materials will be discussed.

2.1 Selective Laser Melting

Selective laser melting (SLM) is one process of powder bed fusion additive manufacturing where the metal powder is spread in a thin layer across the powder bed fed from a hopper. A recoater is then moved across the surface of the build plate to provide a uniform layer of metal powder for the build process. The parameters of the laser source are then programed to selectively melt the powder to form the shapes of the part(s) being built. The laser source will heat the metal powder above its melting temperature and the part will begin to take shape. The powder bed will then move down one layer and the next layer of powder is spread by the recoater and the process is repeated until all layers of the part are built. This process is controlled by a programmed set of build parameters that help define the mechanical and physical properties of the final part. (Trevisan, 2017)

2.1.1 Build Parameters

There are four main regions to any part that is being built, upskin, downskin, contour, and bulk, each of which has its own build parameters to optimize the resulting mechanical properties, microstructure, and surface finish. The different regions with unique build parameters include:

- Upskin - Upward facing side of the part
- Contour - Side of the part
- Downskin - Downward facing side of the part
- Bulk - Interior areas of the part

These regions of the AM SLM part are illustrated in Figure 1.

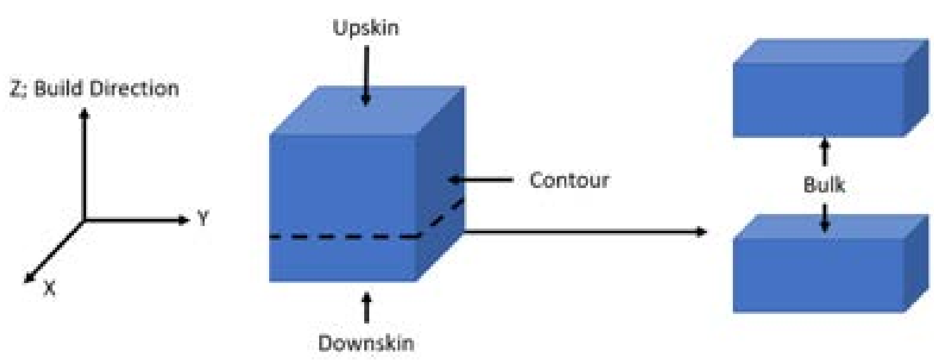

Figure 1 Illustration of regions of AM SLM parts

The target application of the study is an engine piston; therefore, an emphasis will be placed on the contour surface of the part since that directly relates to the sides of the piston. The processing parameters that will be studied are laser power and scanning velocity. These build parameters help define energy density. Energy density on the part being built impacts the mechanical properties, resulting microstructure, and physical properties of the final part. Energy density is given by the equation 2-1.

$$E_d = \frac{P_L}{h_d \times v_s} \tag{2-1}$$

where,

E_d = Energy Density (J/mm^2)

P_L = Laser Power (W)

h_d = Hatching Distance (mm)

v_s = Scanning Velocity (mm/s)

Laser power defines the input radiant energy rate transient supplied by the laser throughout the build process. Hatching distance is the distance between the scan lines of the laser. Scanning velocity is the speed of the laser traversing the powder throughout the build process. (Krishnan, 2014)

Energy density, defined by laser power, hatching distance, and scanning velocity, will have a direct impact on the resulting melt pool geometry of the part. Differences observed in the melt pools suggest different cooling rates that the samples experience. As the energy density is increased the melt pools will become larger, this is due to the high power and/or slow scanning speed of the laser. The large melt pools observed in the samples are caused from preheating of the surface from the previous pass. The melt pool geometry will lead to differences observed in the microstructures and mechanical properties. The increase in energy density will also improve the surface roughness because the melt pools will become more structured and stable allowing for full powder particle melting. (White, 2014)

2.1.2 Metal Powder and Powder Properties

There are many materials that are commonly used for additive manufacturing. These include steel, aluminum, titanium, and nickel alloys. These powders are produced through an atomization process which has a direct effect on the powder properties such as the powder particle size distribution, the shape of the powder, and the chemical composition. These can directly affect the printability of the powder and the flow properties of the powder. For this study, AlSi10Mg will be used to compare to conventional aluminum alloys, AA2618 and AA4032, commonly used in the piston application.

2.2 Targeted Application

The piston set up is a complex system which relies on many different components for the process to be successful. This study investigates the wear response between piston material and cylinder wall material. The motion between these two parts is pure sliding and reciprocating. The cylinder liner is commonly made from an iron alloy. Pistons are usually made from forged or cast aluminum alloys, such as AA2618 which is a low silicon forged aluminum alloy or AA4032 which is a high silicon forged aluminum alloy. Pistons are subjected to extreme temperatures and pressures, therefore, using a high strength, high thermal conductivity, and low mass density material for the piston application is ideal. (Balducci, 2017)

Conventional materials used for pistons are either cast or forged with individual advantages and disadvantages. The casting process is where the alloy is melted and then poured into a mold to create a basic shape. The alloy cools and solidifies inside of the mold and then the mold is removed. The casting is then machined to the final shape. These types of materials provide high durability and are less expensive to produce then forged pistons, however, the resulting cast is not as strong as forged pistons. (Mbuya, 2012)

Forged pistons are created by placing a cast preform in the piston die while it is still hot, and the hydraulic press is then used to shape the material into a rough piston. This is a thermomechanical process which removes the porosity (voids) in the material which causes the grain flow to become directional orienting the grains in a way that increases strength and toughness. This is considered a recrystallization process that promotes grain growth by replacing deformed grains with grains that are free from defects. These types of pistons provide a higher performance and a stronger material than cast pistons because they can handle extended exposures to high temperatures. However, forged pistons are costlier to produce because the initial tooling costs are more expensive than other applications and therefore only used in high performance applications. (Schikorra, 2007)

Lubrication is another aspect of the piston process. It helps in reducing friction, cooling, sealing, cleaning, and providing corrosion protection for all moving parts. Lubricating motor oils contain additives which will allow the oil to work more efficiently for longer periods of time.

An additive manufactured selective laser melted piston would have many benefits over a conventional forged or cast piston. One of the benefits is optimizing the geometry of the AM SLM part by light weighting the current geometry by including more void areas and thinner sections than conventional manufacturing. Currently, additive manufactured components cost more than their conventional counterpart because of the costs of the initial materials, set up, and increased build time compared to conventional means. However, for the high-end performance market the benefit of using additive manufactured selective laser melted parts outweighs the cost due to the potential higher hardness, higher temperature performance, improved mechanical properties, and lighter weight. These higher costs can be offset by more near net-shape part which reduces machining. (Barbieri, 2017)

2.3 Wear Mechanics

Mechanical wear is classified as the gradual removal of a material when two contacting bodies are in motion. The type of wear mechanism observed is dependent on the material properties and the conditions of the application where the wear is occurring. The purpose to understanding how wear impacts the system being studied is to control and limit the wear to improve efficiency and reduce the cost of maintenance and material replacement. In this study piston wear will be simulated to understand how additive manufactured selective laser melted AlSi10Mg samples compare to conventional aluminum alloys.

There are many techniques that are used to determine the wear rate of a material throughout tribology testing including weight measurements, contact profilometry, and non-contact optical profilometry among many others. Weight measurements are used to evaluate the mass wear rate which is the simplest method however, the disadvantage is if there is material transferred during the wear testing. Contact profilometry is used to detect the 2D profile of the wear scar however, this type of characterization cannot be used throughout testing if the sample is not able to be removed from the holder. Non-contact optical profilometry can be used to determine wear rate over time if a setup is used where the sample can move between the wear apparatus and the 3D non-contact optical profilometer. This is used by imaging the samples and calculating width and depth of the tribological wear scars.

2.4 Materials

The AM SLM materials used for this study are made from aluminum alloy AlSi10Mg powder and the conventional aluminum alloys are AA2618 and AA4032.

Aluminum alloy AlSi10Mg is a widely used alloy for additive manufacturing because of its strength, hardness, and melting temperature. This material is used for parts that experience high loads and elevated temperatures. AlSi10Mg is considered a hypo eutectic alloy and is also a hardenable alloy. (Herzog, 2016) The literature composition of AlSi10Mg is in Table 1. (EOS Aluminum AlSi10Mg Material Data Sheet, 2014)

Table 1 Literature compositional analysis of AlSi10Mg (EOS Aluminum AlSi10Mg Material Data Sheet, 2014)

Aluminum	balance
Silicon	9.0 – 11.0 wt. %
Iron	≤ 0.55 wt. %
Copper	≤ 0.05 wt. %
Manganese	≤ 0.45 wt. %
Magnesium	0.2 – 0.45 wt. %
Nickel	≤ 0.05 wt. %
Zinc	≤ 0.10 wt. %
Lead	≤ 0.05 wt. %
Tin	≤ 0.05 wt. %
Titanium	≤ 0.15 wt. %

Silicon is added to AlSi10Mg improve the laser absorption. Since aluminum has a high reflectivity this can reduce the energy of the laser when the laser reflects off the aluminum powder particles. This makes AlSi10Mg metal powder easier to use to produce parts by AM SLM. The percentage of magnesium also needs to be controlled because Mg_2Si precipitates need to form during heat treatment. (Iturrioz, 2018)

AM SLM as built components can have anisotropy therefore, additive manufacturing vendor EOS recommends the parts to be stress relieved. (EOS Aluminum AlSi10Mg Material Data Sheet, 2014) Stress relief is a thermal treatment which can impact mechanical properties of the as built AlSi10Mg part. The higher the stress relief temperature the lower the hardness. This is due to growth of silicon particles which results in an increase in size, also known as Ostwald ripening. (Li, 2016, Iturrioz, 2018)

Table 2 lists room temperature literature mechanical properties for AlSi10Mg in both the x-y build direction and the z build direction. Table 2 also includes as built and post stress relieved mechanical properties. As expected there was a decrease in mechanical properties after the part was stress relieved for 2 hours at 300°C. (EOS Aluminum AlSi10Mg Material Data Sheet, 2014)

Table 2 Literature mechanical properties of AM selective laser melted AlSi10Mg as built and post stress relieved conducted at room temperature (EOS Aluminum AlSi10Mg Material Data Sheet, 2014)

	As Built	Stress Relieved 300°C 2 hours
Tensile Strength (XY direction)	460 MPa ± 20 MPa	345 MPa ± 10 MPa
Tensile Strength (Z direction)	460 MPa ± 20 MPa	350 MPa ± 10 MPa
Yield Strength (XY direction)	270 MPa ± 10 MPa	230 MPa ± 15 MPa
Yield Strength (Z direction)	240 MPa ± 10 MPa	230 MPa ± 15 MPa
Elongation at Break (XY direction)	9% ± 2%	12% ± 2%
Elongation at Break (Z direction)	6% ± 2%	11% ± 2%
HBW 2.5/62.5 (Brinell)	~119 ± 5 HBW	Not Tested

Aluminum alloy AA2618 is a commonly used hypo-eutectic piston alloy. This alloy is generally used in high performance applications and is designed for elevated temperatures; however, the strength and hardness of this material will decline with long term high temperature exposure. The coefficient of thermal expansion for this material is high which means it expands and contracts more easily. Therefore, at low temperatures the piston-to-cylinder clearance is larger than that of other alloys. This property is important to understand because an incorrect piston-to-cylinder fit can cause increased friction, piston damage, and failures. (Novy, 2009) The composition of this material can be seen in Table 3. (Aluminum 2618-T61, 2019)

Table 3 Literature compositional analysis of aluminum alloy AA2618-T61 (Aluminum 2618-T61, 2019)

Aluminum	balance
Silicon	0.10 – 0.25 wt. %
Iron	0.90 – 1.3 wt. %
Copper	1.9 – 2.7 wt. %
Magnesium	1.3 – 1.8 wt. %
Nickel	0.9 – 1.2 wt. %
Zinc	≤ 0.10 wt. %
Titanium	0.04 – 0.10 wt. %

The microstructure of AA2618 includes intermetallic phases that form from the alloying elements iron, nickel, copper, and magnesium. Iron and nickel alloying elements are controlled at a 1:1 ratio to bound them in the intermetallic phase Al_9FeNi, which increases the resistance of the alloy to plastic deformation. If the ratio of iron to nickel is not 1:1 then other intermetallics can form that include copper, iron, and nickel. The copper containing intermetallic phases can reduce the content of copper needed to form Al_2CuMg, which is a strengthening phase of this alloy.

(Novy, 2009, Elgallad, 2014) The room temperature literature mechanical properties for aluminum alloy AA2618 are listed in Table 4. (Aluminum 2618-T61, 2019)

Table 4 Literature mechanical properties for aluminum alloy AA2618-T61 conducted at room temperature (Aluminum 2618-T61, 2019)

Tensile Strength	441 MPa
Yield Strength	372 MPa
Elongation at Break	10%
HBW; 10/500 (Brinell)	115 HBW

Aluminum alloy AA4032 is another material that is commonly forged to produce pistons. It is a high silicon-based material and is considered hyper eutectic. This material has a low coefficient of thermal expansion, so at low temperatures there is a tighter piston to cylinder fit. This property is important to understand because an incorrect piston-to-cylinder fit can cause increased friction, piston damage, and failures. AA4032 aluminum alloy is generally used for high life pistons rather than high performance pistons. This material is highly alloyed to increase its thermal stability with copper, magnesium, and nickel. (Balducci, 2017, Novy, 2009) Table 5 reports the literature compositional analysis of AA4032. (Aluminum 4032-T6, 2019)

Table 5 Literature compositional analysis of aluminum alloy AA4032-T6 (Aluminum 4032-T6, 2019)

Aluminum	balance
Silicon	11.0 – 13.5 wt. %
Iron	≤ 1.0 wt. %
Copper	0.5 – 1.3 wt. %
Magnesium	0.8 – 1.3 wt. %
Nickel	0.5 – 1.3 wt. %
Zinc	≤ 0.25 wt. %
Chromium	≤ 0.10 wt. %

The alloying elements of AA4032 are iron, silicon, magnesium, nickel, and copper which create intermetallic phases including Mg_2Si, Al_2Cu, and Al_2CuMg. The iron alloying element is usually added to enhance the alloy properties at high temperatures, however, it is controlled to a low percentage. The room temperature literature mechanical properties for aluminum alloy AA4032 are listed in Table 6. (Aluminum 4032-T6, 2019)

Table 6 Literature mechanical properties of aluminum alloy AA4032-T6 conducted at room temperature (Aluminum 4032-T6, 2019)

Tensile Strength	379 MPa
Yield Strength	317 MPa
Elongation at Break	9%
HBW 10/500 (Brinell)	120 HBW

3.0 Literature Review

There are many different aspects of the additive manufacturing selective laser melting process that can affect the mechanical properties of the part being built. A literature review was conducted to understand the effect of the processing parameters on mechanical properties and wear performance. As well as understanding the effect of different stress relief temperatures and times and how they can affect the mechanical properties and in turn the affect wear performance. This chapter will summarize the conducted literature review.

3.1 Effect of Processing Parameters on AM Selective Laser Melted Parts

The additive manufactured selective laser melted materials often have higher hardness and finer grains than the same materials that are made with standard conventional methods. This is because of the AM SLM process. The laser heats the materials at such high rates and the material cools rapidly causing the fine grains. The laser processing parameters, power and velocity, will have the highest effect on the heating and cooling of the powder to form the metal part. These settings can influence the melt pool geometries which will in turn change the microstructure and mechanical properties. (Hanzl , 2015, Trevisan, 2017)

Hanzl, et al. have investigated the effect of select build parameters on surface quality and mechanical properties. Observations were made into the laser power, velocity, and scanning speed, to understand what the surface finish is by varying those processing parameters. If the power was not high enough to melt the powder, then the resulting surface will have a large amount of powder that will remain partially melting after the production is completed. If the power is high enough to only partially melt the powder but has a low scanning speed, then the surface of the powder will be fused together but the core of the powder will remain unmelted. This will result in a surface that has what is called the balling phenomenon. The third case is when both the power and velocity are high, this will result in a surface that has long lines which is the powder particles solidifying in the laser path but not fusing the different laser lines together. The final type of processing parameters that is discussed is when the powder experiences complete melting. This means the laser power was high enough to completely melt the powder forming a solid surface with no balling or lines. (Hanzl, 2015)

One study that was reviewed, observed the impact that various processing parameters had on mechanical properties. The direction of the build also impacted the mechanical properties with several angles being observed. These angles were both in relation to the y axis and the z axis. This test demonstrated that the angle at which the sample were built had an impact on the mechanical properties with angles in relation to the z axis on average have better mechanical properties and a reduction in anisotropy in the part. The anisotropy reduction allows for a more uniform mechanical properties in various orientations. (Hanzl, 2015)

Another study considered the impact of various processing parameters and build strategies on the resulting microstructure, mechanical properties, and physical properties. One study looked at the effect of how the powder melted and solidified during the process and how that affected the resulting microstructure. A cellular dendritic structure is observed throughout the part however, that structure changes depending on the thermal gradients throughout the part, meaning the processing parameters used to build the part will influence heating and cooling within the part itself and will change the microstructure. (Trevisan, 2017)

Researchers discussed how the processing parameters will affect the mechanical properties of the material, looking specifically into varying the power and velocity build parameters. These varying build parameters yielded similar tensile testing UTS however, the presence of pores, the grain orientation, and texturing of the grains impacted the elongation at break and the fracture point. (Trevisan, 2017)

One study that was observed was looking at the effect of laser power, velocity, and hatch spacing on Brinell hardness and density of the material. Increasing laser power increased hardness, the increasing velocity decreased hardness, and the increase in hatching distance decreased hardness. These same observations can also be observed with density. This demonstrates that there is an optimal combination of processing parameters for both physical and mechanical properties. (Krishnan, 2014)

3.2 Wear Performance of Additive Manufactured Parts

There have been a series of sliding and fretting wear tests completed on as built additive manufactured selective laser melted samples, samples that were annealed at different temperatures, and conventionally made aluminum alloys. The types of wear tests performed on the aluminum materials reviewed in the paper were mostly dry sliding wear testing at low loads and low speeds and analyzed throughout the wear process. (Zhu, 2018)

All the testing concluded that the wear rate is inversely proportional to the mechanical properties, which means the higher the hardness and tensile properties the lower the wear rate is. This is due in part by the finer grains and the alloying materials of the additive manufactured selectively laser melted parts which create intermetallic particles. (Zhu, 2018)

The annealing temperatures also lowered the tensile and hardness mechanical properties. Also the higher the annealing temperature the lower the mechanical properties were, which directly relates to the wear resistance. The annealing temperature promoted an increase in the growth of silicon particles. This caused the mechanical properties to decrease and therefore the wear properties decreased. (Zhu, 2018)

The effect of heat treatment parameters was completed in two different studies looking at as built samples and heat treated samples at various temperature, of AlSi10Mg aluminum alloy built by AM SLM. Both studies had concluded that the heat treatment of the samples significantly reduced the tensile properties and the hardness values when compared with the as built material. The study concluded the higher the heat treatment temperature the lower the mechanical properties will be, specifically testing hardness and tensile properties. The reason for the decrease in the mechanical properties was from Ostwald ripening. Ostwald ripening is the combination of small silicon particles which results in an increase in size of silicon particles and a decrease in the number of silicon particles. Therefore, the higher the stress relief temperature the lower the hardness will be because the increase in silicon particles causes the mechanical properties to decrease. Silicon is the strengthening alloying element in AlSi10Mg. (Han, 2019, Li, 2016, Iturrioz, 2018)

Another study investigated the effect of laser power on microhardness and wear rate. This study observed that the wear rate decreased as the laser power increased and consequently the microhardness increased as the laser power increased. However, the highest laser power that was tested had a significant drop in microhardness and the wear rate significantly increased. (Kang, 2016)

The same study looked at how the laser power affected the microstructure of the samples of hypereutectic aluminum silicon alloys by AM SLM. As the laser power was increased the porosity of the AM SLM samples decreased and the morphology of the pores changed from asymmetrical to spherical. The increase in laser power also affected the morphology of the silicon particles also changing them from asymmetrical to spherical and removing any nano silicon particles present. The wear rate shows that an increase in laser power decreases the wear rate except for the highest laser power. The highest laser power also had the lowest hardness values of the test. (Kang, 2016)

3.3 Critical Questions

There are still some critical questions after completing the literature search that should be considered while moving through the research. How do additional build parameters besides laser power, velocity, and hatching distance affect the mechanical properties, microstructure, and tribological wear performance? Even though this study will be focusing on the build parameters that affect energy density, there are many other parameters that should be considered to further improve the mechanical properties, microstructure, surface finish, and tribological wear performance. How does grain structure and grain orientation affect the wear mechanics? While completing the literature search a common theme emerged suggesting a finer grain structure would improve the wear performance of the material, but it would be interesting to note if there are other grain structures and orientations that may provide some improved wear performance. Are there other mechanical properties that should be considered that may impact the wear performance or the wear scar evolution? A more in depth review should be conducted to fully understand the wear mechanics of the materials.

4.0 Research Description

4.1 Hypothesis

The hypothesis of the present investigation is that the wear performance of aluminum alloys can be optimized using SLM additive manufacturing, particularly using increased energy density to achieve a fine grain structure resulting in high hardness and high wear resistance defined by the Hall Petch equation. By adjusting build parameters of the AM SLM process, the resulting components can have different resulting microstructures, porosities, and surface roughness parameters which further modify wear resistance. While additive manufacturing is known to produce parts with high roughness in their as-printed state, surface finishing techniques can be used to reduce surface roughness parameters to eliminate this factor. The basis of these hypotheses is prior literature which suggests a strong connection between build parameters and resultant mechanical and physical properties. (Kang, 2016)

4.2 Objectives

The present research was conducted through four objectives. One objective of this study is to investigate the material properties of AM SLM AlSi10Mg samples post stress relieved with four different build parameter sets in comparison to conventional materials used in piston application. Another objective is to surface finish the samples by polishing them to a roughness between 0.2 μm and 0.5 μm and to complete a comparison of surfaces by non-contact 3D optical profilometry and contact profilometry. The third objective is to analyze the wear mechanics of the post stress relieved AM SLM surfaces, the surface finished AM SLM samples, and the conventional aluminum alloys to compare the wear mechanics and to determine if there are any advantages or disadvantages to any of the samples. Last of all, to draw conclusions and determine relationships between the different forms of testing based on the material properties and the wear mechanics.

4.3 Tasks

The first task was to understand the mechanical and physical properties of the conventionally made AA2618 and AA4032 samples as well as the additively manufactured AlSi10Mg with the different build parameters and surface finishing techniques. This included several different tests such as Archimedes' density, inductively coupled plasma analysis, Vickers hardness, Rockwell B hardness, scanning electron microscopy, energy dispersive spectroscopy analysis, electron backscatter diffraction, and surface finish analysis. The next task was to surface finish the samples to 0.2 μm to 0.5 μm surface roughness and complete a comparison of the surface roughness parameters. The third task was to determine the wear mechanics of the samples tested on a tribometer with the conditions that a pistons experiences and understand the surface roughness and the wear scar appearance of the samples before and after the wear testing. The forth task was understanding if build parameters or surface finishing techniques effect the properties and wear mechanics of the samples. Finally, discussing the potential benefit of using AM SLM AlSi10Mg samples over conventional aluminum alloys.

5.0 Experimental Details

5.1 Samples

5.1.1 Additive Manufacturing Selective Laser Melting Build Information

Two different prints of AlSi10Mg samples were completed for this study, one build using an EOS M290 (print 1) and the other build using an EOS M400 (print 2). Both machines were equipped with a 400 W laser with a beam diameter (spot size) of 80 μm, and the builds were made with a build plate temperature of 100°C to minimize thermal stresses. The samples were built in a nitrogen atmosphere to reduce the oxygen contact and reduce the possibility of the formation of oxides in the printed parts. The samples were then stress relieved for 2 hours at 300°C. The bulk of the sample is built with the Conventional Slow build parameters with just the few layers closest to the contour surface having the contour build parameter differences reported in Table 7. Conventional Slow build parameters are literature values. (Bartolo, 2013) The calculated energy density for the different samples from lowest energy density to highest energy density is: Conventional Slow = Conventional Fast < Proprietary Low < Proprietary High.

Since pistons are the targeted application the wear resistance of the contour side is investigated using build parameters to modify the microstructure, physical and mechanical properties, and surface topography.

Table 7 Build parameters used to print contour surfaces for this research

	Print	Layer Thickness	Contour Power	Contour Velocity	Hatch Spacing	Calculated Energy Density
Conventional Slow (CS)	Print 1	0.03 mm	80 W	900 mm/s	0.19 mm	0.47 J/mm^2
Conventional Fast (CF)	Print 2	0.03 mm	210 W	2360 mm/s	0.19 mm	0.47 J/mm^2
Proprietary Low (PL)	Print 1	0.03 mm	Arconic Proprietary	Arconic Proprietary	0.19 mm	Energy Density Increased from Conventional Slow and Conventional Fast
Proprietary High (PH)	Print 1	0.03 mm	Arconic Proprietary	Arconic Proprietary	0.19 mm	Energy Density Increased from Proprietary Low

5.1.2 AlSi10Mg

AlSi10Mg samples were cuboid in shape, as shown in Figure 2. The samples were printed with two builds. Print 1 was built on the EOS M290 with AlSi10Mg powder lot 1 for Conventional Slow, Proprietary Low, and Proprietary High. Print 2 was built on the EOS M400 with AlSi10Mg powder lot 2 for Conventional Fast. Both AlSi10Mg powder lots were received from EOS. The contour face is the testing face for the AlSi10Mg samples.

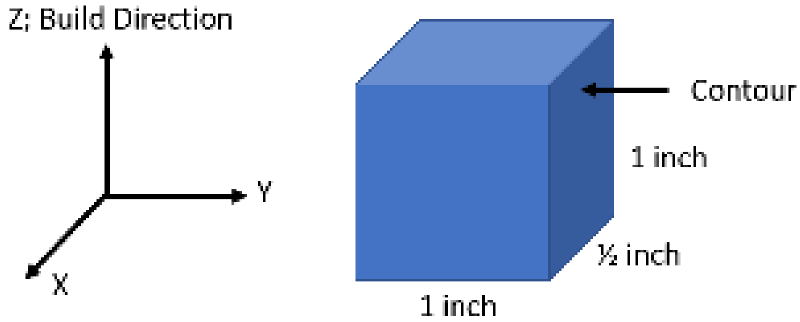

Figure 2 Schematic of sample orientation AM SLM AlSi10Mg showing part dimensions and test surface (contour face)

Figure 3 displays the particle size distribution for powder lot 1 and powder lot 2. Powder lot 1 Gaussian distribution was centered on 44.02 µm, D10 26.81 µm, D50 41.67 µm and D90 64.36 µm. Powder lot 2 the Gaussian distribution was centered on 46.88 µm, D10 27.81 µm, D50 44.13 µm, and D90 69.49 µm. Both powder lots show a positively skewed Gaussian distribution.

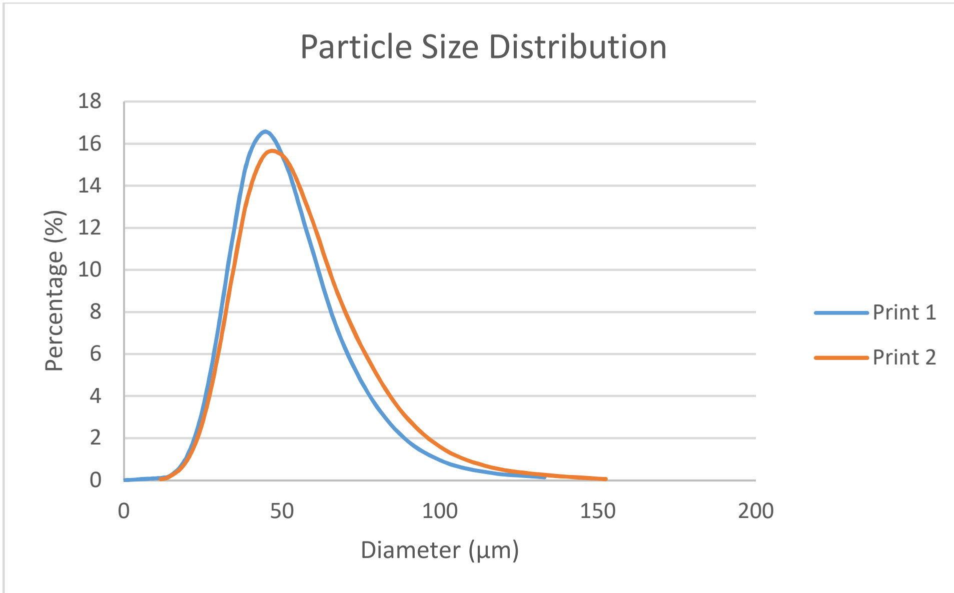

Figure 3 Particle size distribution for print 1 and print 2 of AlSi10Mg powder

5.1.3 Aluminum Alloy AA2618-T6511

A 3 in. diameter heat treated extrusion of aluminum alloy AA2618-T6511, supplied by Arconic, was used for comparison. The temper designation denotes the material was solution heat treated, artificially aged, permanent set (minimal stretching), and straightened. The sample was sliced into 5 mm thick discs and the testing was conducted on the outer perimeter of the sliced face. Extrusion is a thermomechanical forming process which significantly increases the mechanical properties of the material. The extrusion process and the heat treatment T6511 will increase the mechanical properties. Figure 4 demonstrates the sample orientation for this investigation.

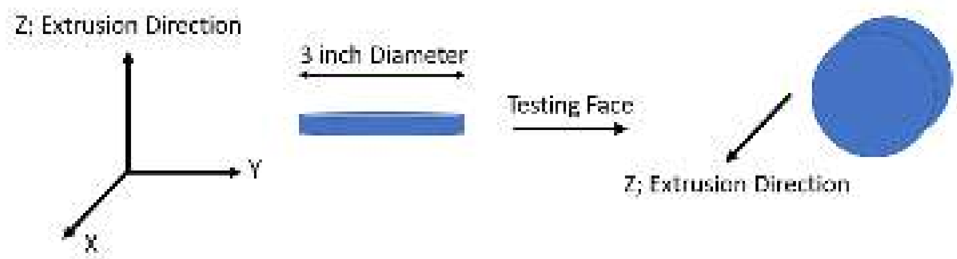

Figure 4 Schematic of sample orientation of AA2618 showing part dimension and test face

5.1.4 Aluminum Alloy AA4032-T651

Aluminum alloy AA4032-T651 extrusion, purchased from Eagle Alloys, is used for testing, which was a 1 in. diameter rod that was 36 in. long. The temper designation denotes the material was solution heat treated, artificially aged, and permanent set (minimal stretching) to remove residual stresses. The sample was sliced into 30 mm thick discs and the testing was conducted on the outer perimeter of the sliced face. Extrusion is a thermomechanical process which significantly increases the mechanical properties of the material. The extrusion process and the heat treatment T651 will increase the mechanical properties. Figure 5 demonstrates how the same was oriented for testing.

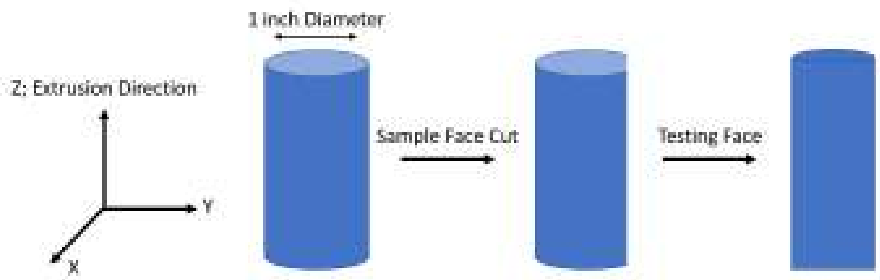

Figure 5 Schematic of sample orientation of AA4032 showing part dimension and test face

5.1.5 Surface Finishing Sample Preparation

Since build parameters affect contour surface roughness wear studies were conducted on the post stress relieved and the surface finished samples. The samples were surface finished to eliminate surface roughness as a confounding factor in the tribology testing. The surface finished samples were polished with silicon carbide (SiC) abrasive papers having progressively finer abrasive size (120, 240, 600, 800, 1200 grit) to a final surface roughness between 0.2 µm and 0.5 µm. All of the samples were polished on a new set of abrasive paper until the previous polishing lines were visually removed from the surface. The average amount of material removed from the samples was between 250 µm to 350 µm.

5.2 Physical Properties

5.2.1 Inductively Coupled Plasma

Inductively coupled plasma (ICP) analysis is a technique that can determine concentration of alloying elements. A multistep method is used for sample preparation in order to dissolve the solid material. The first step is to initiate a reaction with the metal using a 20% NaOH solution in distilled deionized (DDI) water. After dissolution is complete, a 30% H_2O_2 solution is added and evaporated to dryness. The next step is to acidify and oxidize the solution by adding DDI water, warming the sample until the contents are dissolved, and then cooling it. Then slowly add a 50% solution of HNO_3, followed by a 50% solution of HCl, and 30% H_2O_2. The mixture is then heated to drive off the peroxide. Cobalt is added to the mixture for an internal standard.

5.2.2 Archimedes' Density

The densities of post stress relieved specimens were measured to determine differences in porosity. The auxiliary liquid used in this testing is 200 proof ethanol because its surface tension is lower than water to minimize bubble formation that would lead to density measurement errors. Table 8 reports the surface tension differences between water and ethanol. (Ethanol, 2016, Water H_2O, 2019)

Table 8 Surface tension of water and 200 proof ethanol (Water H_2O ,2016, Ethanol, 2016)

Liquid	Surface Tension at Room Temperature
Water	72 dynes/cm
Ethanol, 200 Proof	22 dynes/cm

The temperature of ethanol, the ambient temperature, and humidity are all recorded for accurate density calculation. The sample is weighed outside of the ethanol, then it is submerged in ethanol, and the weight is recorded again. Density is calculated based on weight measurements and calibrated standards, which is a NIST certified silicon standard and an aluminum control. Repeated measurements were made for each sample for accuracy.

5.3 Mechanical Properties

5.3.1 Vickers Hardness

Vickers hardness is an indentation test in which a square-based pyramidal diamond indenter having specific face angles is forced under specific conditions into the surface of the test sample. After removal of the test force, the length of the two diagonals of the area created from the Vickers indenter are measured to calculate the Vickers hardness number.

The samples were cross sectioned, so the contour edge can be observed. They were then mounted in KonductoMet in 1.5 in. diameter mounts and polished with the procedure in Table 9.

Table 9 Polishing procedure for Vickers hardness mounted samples

Step	Abrasive/Cloth	Force (N)	RPM	Time
1	120 Grit Silicon Carbide Paper	10	300	Until Planed
2	320 Grit Silicon Carbide Paper	10	150	30 seconds
3	600 Grit Silicon Carbide Paper	10	150	30 seconds
4	3 micron/mol	20	150	2 minutes
5	3 micron/silk	25	150	3 minutes
6	1 micron/mol	20	150	2 minutes
7	1 micron/silk	25	150	3 minutes
8	0.05-micron OPS Colloidal Silica	25	150	30 seconds

Hardness measurements were then taken following ASTM E92-17, "Standard Test Method for Vickers Hardness and Knoop Hardness of Metallic Materials." Figure 6 shows the locations of the indents performed. Five indents were performed in the center to get bulk properties and five indents were performed on the cross section edge to get surface properties. All testing was Vickers scale HV 0.1 with a test force of 100 gf. All indents are 0.2 mm away from each other and the edge to reduce any chance of edge effects and interactions between the indents. Vickers tip is tested with the calibrated standard to verify it is compliant. (ASTM Standard E92, 2017)

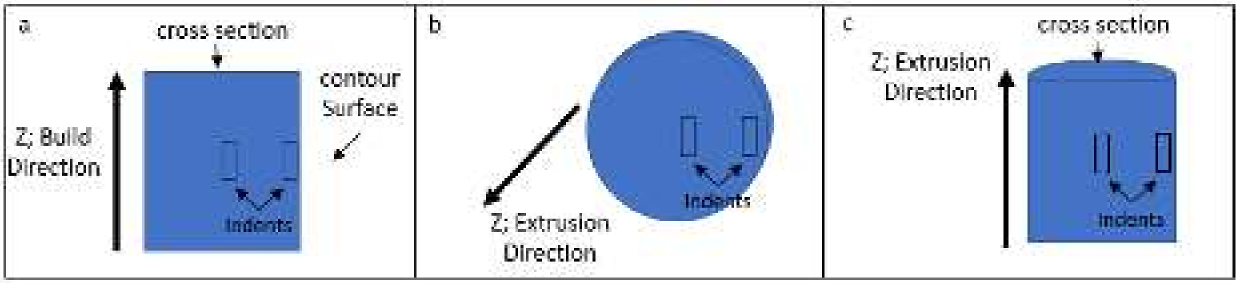

Figure 6 Vickers hardness indent locations a.) AM SLM samples CS, CF, PL, and PH b.) AA2618 c.) AA4032

5.3.2 Rockwell B Hardness

Rockwell B hardness testing was performed using ASTM E 18-19 "Standard Test Methods for Rockwell Hardness of Metallic Materials." The Rockwell Hardness test consists of the instrument loading the sample to a fixed minimum load, increasing that load to a maximum load, and then unloading to the fixed minimum load. The differences between the depth of the first minimum load and the depth of the second minimum load are used to calculate hardness.

Rockwell B hardness for aluminum samples used in this study is standardized with the following settings: 0.0625 in. (1.588 mm) tungsten carbide ball, initial and final minimum test force 10 kgf, and total (maximum) test force 100 kgf. Rockwell B hardness is calculated with the equation 5-1 and 5-2.

$$Rockwell\ Hardness\ B = 130 - \frac{h}{0.002} \tag{5-1}$$

(5-2)

$$h = Final\ Depth\ Measurement - Baseline\ Depth\ Measurement$$

After measuring a calibrated standard, three measurements were taken on the surface and on the cross section of the bulk. All indents are at least 2.5 times the diameter of the tungsten carbide ball spaced from each other and the edge to reduce any chance of edge effects and interactions between the indents. Rockwell indent locations can be seen in Figure 7.

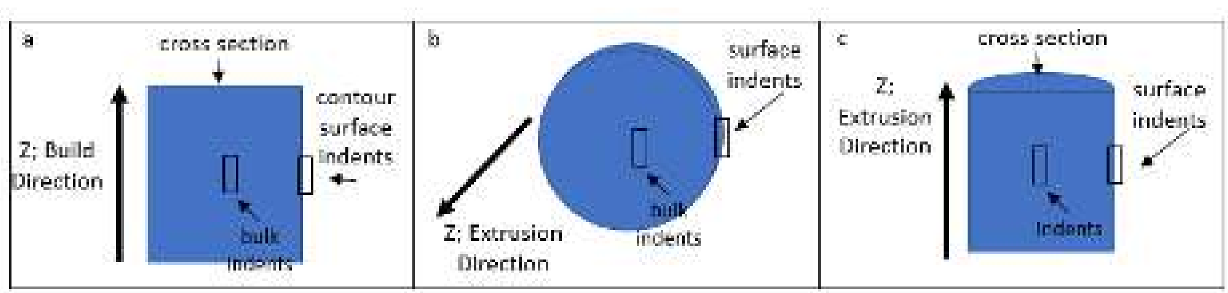

Figure 7 Rockwel B hardness indent locations a.) AM SLM samples CS, CF, PL, and PH b.) AA2618 c.) AA4032

5.4 Microstructure

5.4.1 Optical Microscopy

Optical microscopy was used to observe the melt pools geometries on the cross sectioned contour surfaces (see schematic, Figure 6a) of the additive manufactured selective laser melted samples in the post stress relieved condition and the post stress relieved surface finished condition.

The samples were cross sectioned and mounted in 1.5 in. mounts with transoptic powder from Beuhler. The samples were then polished with the procedure outlined in Table 10.

Table 10 Polishing procedure for mounted samples

Step	Abrasive/Cloth	Force (N)	RPM	Time
1	120 Grit Silicon Carbide Paper	10	300	Until Planed
2	320 Grit Silicon Carbide Paper	10	150	30 seconds
3	600 Grit Silicon Carbide Paper	10	150	30 seconds
4	3 micron/mol	20	150	2 minutes
5	3 micron/silk	25	150	3 minutes
6	1 micron/mol	20	150	2 minutes
7	1 micron/silk	25	150	3 minutes
8	0.05-micron OPS Colloidal Silica	25	150	30 seconds

The mounted samples were etched for 10 seconds in Graff-Sargent to highlight the melt pool geometries. The samples were imaged at different magnifications to observe the melt pool geometries.

5.4.2 Electron Backscatter Diffraction

Electron backscatter diffraction (EBSD) is a technique performed in a scanning electron microscope (SEM) to study crystallographic orientation of individual grains. This technique quantifies the crystallographic texture and can be used to study grain size, defects, and deformation of the microstructure.

The samples were cross sectioned and mounted in KonductoMet. The mounts were 1.5 in. in diameter and were polished with the procedure outlined in Table 10.

EBSD analysis was run on an XL 30 SEM on the cross sectioned surfaces (Figure 6). The working distance was 16 mm to 18 mm, the spot size was 5, the accelerating voltage was 20 eV, and the tilt was 70°.

5.4.3 Scanning Electron Microscope

SEM was used is to determine the microstructure of the samples. The scanning electron microscope (SEM) instrument uses a focused beam of electrons which generate signals from the surface of a solid sample. These signals include information about chemical composition, morphology, crystalline structure, and grain orientation. (Scanning Electron Microscopy, 2017)

Samples were cross sectioned and mounted in KonductoMet using a mounting press and the mounts were 1.5 in. in diameter. Samples were then polished with the procedure in Table 10.

SEM analysis was run on an XL 30 SEM on the cross section contour surface and the bulk with various magnifications. The working distance was 8 mm to 10 mm. A scanning electron microscopy-energy dispersive spectroscopy (SEM-EDS) spot and area analysis was used to evaluate the elements present. At least 2 spots and 1 area were analyzed for each sample.

5.5 Surface Properties

5.5.1 Contact Profilometry

A contact profilometer, Mahr stylus instrument, was used to measure surface roughness. The samples were tested in the post stress relieved and the post stress relieved surface finished conditions. Three traces were made using a 2 μm diameter stylus diamond tip in the transverse, $Ra\text{-}T_{avg}$ (μm), and longitudinal, $Ra\text{-}L_{avg}$ (μm), directions. The transverse direction is perpendicular to the build direction and the longitudinal direction is parallel to the build direction. The total trace length is 5.6 mm, omitting the first and last 0.8 mm from the analysis. The data was then filtered through Omnisurf software with the L_s filter at 2.5 μm to remove instrument noise and the L_c filter at 0.8 mm to remove waviness from the sample.

5.5.2 Non-Contact Optical Profilometry

Two instruments were used in this study for the non-contact optical profilometry analysis. Alicona instrument that uses focus variation to form the images. This technique combines both vertical scanning and small depth focus to produce the 3D image which allows the instrument to be able to capture high slope angles. (Alicona, 2019) This technique allows for analysis of additive manufactured selective laser melted samples because of the unmelted powder particles that can be observed on the surface of the post stress relieved samples.

To capture a surface roughness of the post stress relieved samples a stitched image was taken so that the field of view was large enough to get the correct calculated surface roughness. The samples were measured using a stitched image technique with the 20x objective. The specifications for the 20x objective is given in Table 11.

Table 11 Non-contact optical profilometry Alicona insrument 20x objective specifications

Field of View Single Image	0.81 mm x 0.81 mm
Pixels in Field of View	1840 x 1840
Micron per Pixel	0.44

The Zescope uses vertical scanning interference to form the image. In other words, it relies on diffraction and interference to help build the topography image, using fringes. (Zescope Optical Profiler Combines 3D Surface Metrology with Ease of Use, 2009)

This method was used to capture the surface finished samples before the tribological wear experiment, using the 10x objective and a stitched image technique. For the stitched images, the images are overlapped by 30% for proper alignment. The 10x objective specification is given in Table 12.

Table 12 Non-contact optical profilometry Zescope instrument 10x objective specifications

Field of View Single Image	0.89 mm x 0.67 mm
Pixels in Field of View	1392 x 1040
Micron per Pixel	0.64

The captured image is filtered with a L_s filter of 2.5 μm to remove instrument noise and a L_c filter of 0.8 mm to remove waviness from the images. These filtered are comparable to the filters that are used in the stylus profilometry method. The surface parameters that are then generated are transverse roughness, Ra-T_{avg} (μm), perpendicular to the build direction, longitudinal roughness, Ra-L_{avg} (μm), parallel to the build direction, and 3D surface roughness, Sa (μm) which considers all directions and calculates an overall surface roughness.

5.6 Reciprocating Tribology Experiment

The tribology experiment was dry sliding ball on specimen wear testing performed in a reciprocating configuration on the post stress relieved and surface finished samples under an ambient environment. The surface finished samples were polished according to the procedure in section 5.1.5. A 9.5 mm stainless steel 304 ball was loaded against the specimen with a constant load of 10 N. The velocity used for testing was 1 hertz using a 15 mm stroke length. The samples were tested and imaged for 5 minutes, 10 minutes, 20 minutes, and 40 minutes for a total sliding distance of 9 m, 18 m, 36 m, and 72 m respectively. Testing was repeated four times and then calculated data was averaged.

Surface profiles of the wear tracks obtained using a non-contact optical profilometer were used to evaluate the volume loss of the samples and to evaluate the material transferred to the ball. Wear scar volume is calculated with the equation 5-3. (Fildes, 2018)

$$V = \pi * d^2 * \left(r - \frac{d}{3}\right) \tag{5-3}$$

where,

V = wear scar volume (mm^3)

d = depth (mm)

r = radius (mm)

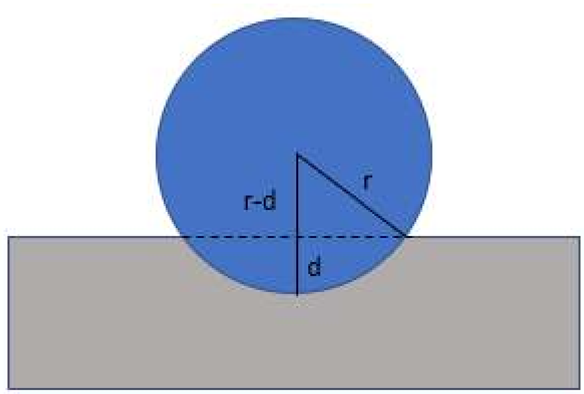

Figure 8 Wear volume calculation diagram

Equation 5-3 is found using Figure 8. Wear rates were then calculated as the ratio of volume loss (mm^3) and the product of total sliding (m) and applied load (N) according to the Archard equation. (Kauzlarich, 2001) The Archard equation is listed in 5-4.

$$k = \frac{V}{F * s} \tag{5-4}$$

where,

k = wear coefficient (mm^3/Nm)

F = normal load (N)

s = sliding distance (m)

6.0 Results and Discussion

The additive manufactured selective laser melted samples will be referred to as follows:

- Conventional Slow – CS
- Conventional Fast – CF
- Proprietary Low – PL
- Proprietary High – PH

Refer to Table 7 in section 5.1.1 for the build parameters.

6.1 Physical Properties

6.1.1 Inductively Coupled Plasma

Inductively coupled plasma (ICP) analysis was completed on the two AlSi10Mg powders, the four additive manufactured selective laser melted samples, and the two conventional aluminum alloys. This analysis was used to confirm that the chemical compositions of the materials used in the study were within the published material limits.

There is no significant difference in the composition of the two AlSi10Mg powders or the AM SLM samples. Analysis reported that the AlSi10Mg powders and the AM SLM samples had weight percentages of all elements that were within the published material limits.

AA2618 sample has similar alloying elements of silicon, magnesium, and iron with low levels of silicon, 0.23%, reinforcing that this is a hypo eutectic aluminum alloy, 1.6% magnesium, and 0.99% iron. Analysis showed that the weight percentages of the elements were within the published material limits.

The AA4032 sample is hyper eutectic with silicon levels of 12.5%. AA4032 is also alloyed with magnesium and iron at 1.1% and 0.17% respectively. Unlike AlSi10Mg, it is also alloyed with copper and nickel. Iron is added in low amounts to enhance the high temperature properties. The copper and nickel additions allow for copper and nickel intermetallics to form. ICP analysis has shown that all elements are within the published material limits.

Table 13 Inductively coupled plasma (ICP) results of post stress relieved AM SLM samples and conventional aluminum alloys

	Al (%)	Si (%)	Fe (%)	Mg (%)	Cu (%)	Ni (%)
AlSi10Mg Powder Print 1	Balance (~89.0)	10.0	0.13	0.39	<0.01*	<0.01*
AlSi10Mg Powder Print 2	Balance (~89.0)	10.0	0.11	0.37	<0.01*	<0.01*
AlSi10Mg CS	Balance (~89.0)	10.0	0.20	0.32	<0.01*	<0.01*
AlSi10Mg CF	Balance (~89.0)	9.94	0.12	0.37	<0.01*	<0.01*
AlSi10Mg PL	Balance (~89.0)	9.94	0.12	0.32	<0.01*	<0.01*
AlSi10Mg PH	Balance (~89.0)	9.96	0.12	0.29	<0.01*	<0.01*
AA2618	Balance (~89.0)	0.23	0.99	1.6	2.6	1.0
AA4032	Balance (~89.0)	12.5	0.17	1.1	1.0	0.76

*data is less than the reporting limit of the element

6.1.2 Archimedes' Density

Archimedes' density was measured to understand the porosity of the AlSi10Mg AM SLM samples. The density measurements indicated that the four AM SLM samples all had lower density than the theoretical maximum of AlSi10Mg. (Zygula, 2018) The percent porosity was then calculated based on the theoretical density and the measured density. Conventional Slow, Proprietary Low, and Proprietary High had a calculated porosity of 0.86% and Conventional Fast had a calculated porosity of 1.34%. Archimedes' density measurements and the calculated percent porosity is reported in Table 14.

Porosity can form a few different ways. They can be due to insufficient energy being delivered to the powder particles during the building process which could be caused by a loss in laser beam energy due to the reflectively of the aluminum in the metal powder. The alloying element of silicon helps to improve laser absorption since aluminum has high reflectivity. Another way pores can form is by the entrapment of gas bubbles in between the layers of the build causing the pores to form. The balling phenomena is a way pores can form which occurs when the energy that is delivered to the build to create the melt pool is too small or the amount of time the laser is on a spot is too short. (Maamoun, 2018) The increased porosity in Conventional Fast could be a result of the balling phenomena since the velocity of the laser is at 2390 mm/s which is significantly higher than the Conventional Slow which is 900 mm/s. Therefore, a lower scan speed can lead to a denser as built part.

Table 14 Archimedes' density results of post stress relieved AM SLM samples compared to the theoretical density (Zygula, 2018)

Sample	Theoretical Density (g/mL)	Average Density (g/mL)	Standard Deviation (g/mL)	Percent Porosity (%)
AlSi10Mg CS	2.68	2.657	0.00058	0.86
AlSi10Mg CF	2.68	2.644	0.00153	1.34
AlSi10Mg PL	2.68	2.657	0.00058	0.86
AlSi10Mg PH	2.68	2.656	0.00058	0.86

6.2 Mechanical Properties

Vickers hardness measurements were completed on the bulk of the sample and the cross sectioned contour surface of the samples as shown in Figure 6. Vickers hardness results showed that the conventional samples AA2618 and AA4032 had average Vickers hardness values of 141 HV and 124 HV respectively, which were significantly higher than the additive manufactured selective laser melted samples as shown in Figure 9. The AM SLM samples all had similar average Vickers hardness values with Conventional Slow, Conventional Fast, Proprietary Low, and Proprietary High exhibiting average hardness values of 83 HV, 85 HV, 83 HV, and 79 HV respectively which can be observed in Figure 9. The differences observed between the bulk and the cross section contour surface are not significant. Error bars in the graphs represent standard deviation.

Rockwell hardness B was tested on the samples on the post stress relieved surface and bulk of the sample as shown in Figure 7. Rockwell hardness B testing was completed on the post stress relieved surface of the AM SLM samples. The average hardness values for Conventional Slow, Conventional Fast, Proprietary Low, and Proprietary High were 26.8 HRB, 26.4 HRB, 25.2 HRB, and 35.7 HRB respectively. This data can be observed in Figure 10. Rockwell hardness B was also tested on the surface finished surface of the AM SLM samples and the conventional samples. This data can be observed in Figure 11. The conventional samples average hardness values were 79.7 HRB for AA2618 and 76.6 HRB for AA4032. The AM SLM samples average hardness values for Conventional Slow, Conventional Fast, Proprietary Low, and Proprietary High were 26.8 HRB, 26.4, 25.2 HRB, and 35.8 HRB respectively. The differences observed in the bulk versus the surface measurements are not significantly different from each other. Error bars in the graphs represent standard deviation.

The same trends are observed in both hardness measurements with the conventional AA2618 and AA4032 samples having a higher hardness than the AM SLM samples. The AM SLM samples all have similar hardness values. Although the AM SLM samples have a finer grain structure they do not have a high hardness than the conventional materials. As discussed in section 5.1, the thermomechanical processing and alloy composition of these materials are selected to optimize the mechanical performance of these alloys through a combination of hot and cold work and the strengthening phase formation.

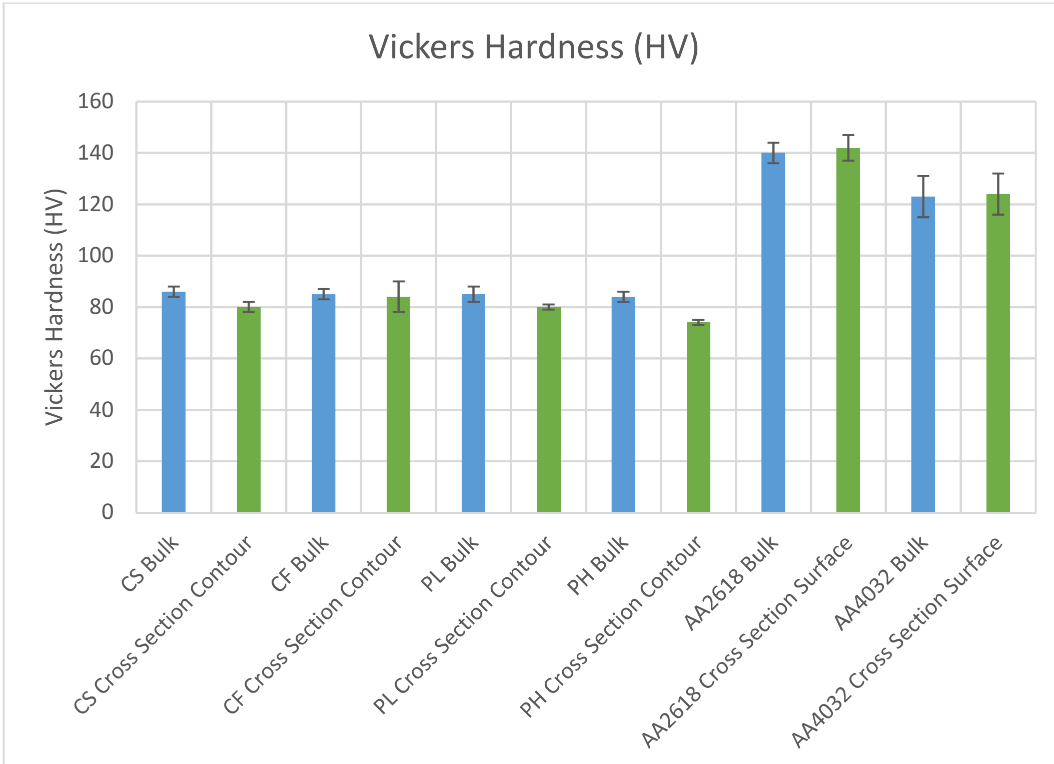

Figure 9 Vickers hardness results for bulk and cross section contour surface of post stress relieved and post stress relieved surface finished AM SLM samples and conventional aluminum samples

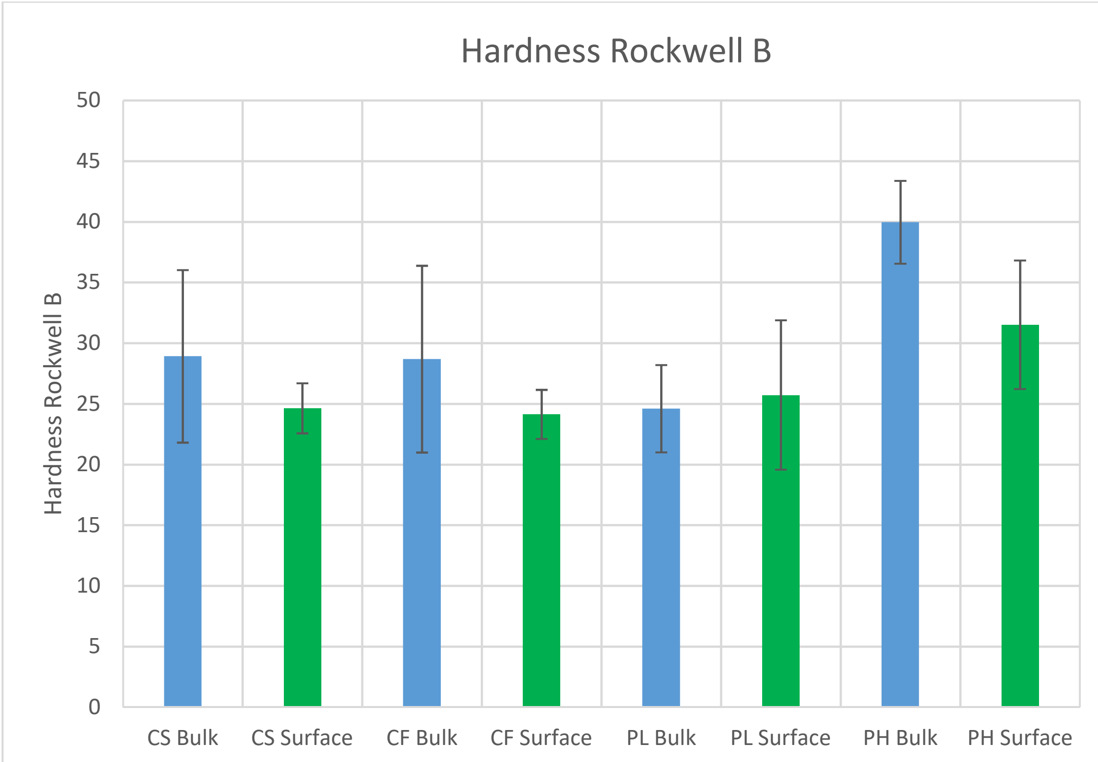

Figure 10 Rockwell B hardness results for bulk and cross section contour surface of post stress relieved AM SLM samples

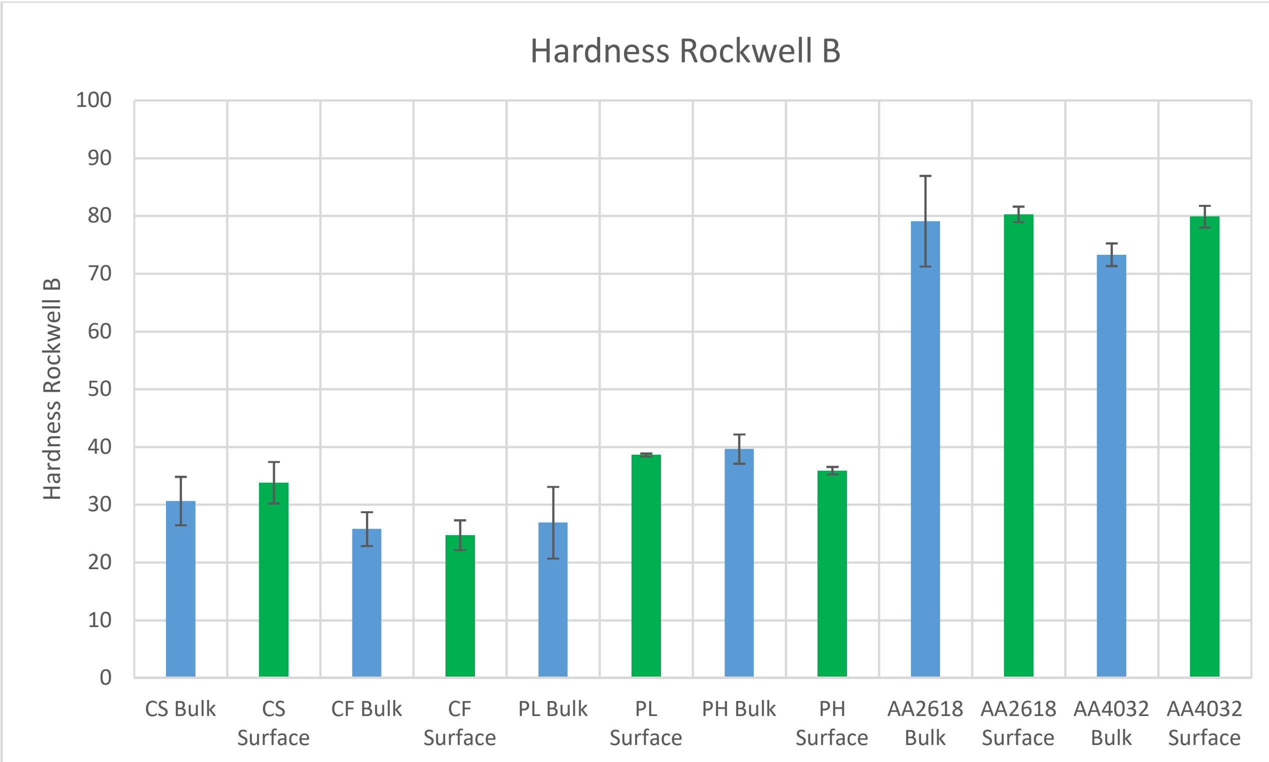

Figure 11 Rockwell B hardness results for bulk and cross section contour surface of post stress relieved surface finished AM SLM samples and conventional aluminum alloy samples

A hypothesis of this investigation was that additive manufactured selective laser melted materials are known to have a higher hardness than conventional materials which in turn can provide improved wear resistance. However, Vickers hardness and Rockwell B hardness testing reports the AM SLM samples having lower hardness values compared to conventional AA2618 and AA4032 samples as observed in Figure 9, Figure 10, and Figure 11. Recommendation by EOS to remove anisotropy is to stress relieve the as built parts at 300°C for 2 hours. Following this recommendation reduces the hardness of the material which in turn can reduce wear performance. There is literature evidence that suggests that heat treatment of AM SLM AlSi10Mg lowers the mechanical properties over the as built condition.

Two studies of heat treatments performed at 450°C to 550°C concluded that the heat treated samples had significantly lowered hardness and tensile strength when compared with the as built material. Both studies observed an increase in size and a decrease in the number of silicon. (Han, 2019, Li, 2016, Iturrioz, 2018)

Future studies may want to investigate the impact of stress relief temperatures on hardness and its resulting impact on wear performance, including as built samples with no stress relief. Mechanical properties in various orientations should also be tested to understand the impact of anisotropy. The microstructure of the materials should also be investigated to understand the evolution of it at different stress relief temperatures when compared to the as built no stress relief state.

To confirm the impact of stress relief a study of hardness was completed using AlSi10Mg Conventional Slow samples that were stress relieved at three temperatures, 250°C, 270°C and 300°C for 2 hours. As expected the higher the stress relief temperature the greater the hardness reduction. This can be observed with the Vickers hardness and Rockwell B hardness results.

Vickers hardness (HV 0.1) was measured as shown in Figure 12. Vickers hardness results of stress relieved temperature study demonstrated that the samples stress relieved at 250°C had a higher hardness than the samples stress relieved at 270°C and 300°C. Vickers hardness results were 106 HV at 250°C, 99 HV at 270°C, and 86 HV at 250°C which are portrayed in Figure 12. Rockwell B hardness was 48.7 HRB for 250°C, 40.0 HRB for 270°C, and 30.7 for 300°C which can be seen in Figure 13. Therefore, the increase in stress relief temperature decreases the hardness of the samples which could be caused by Ostwald ripening. (Han, 2019, Li, 2016)

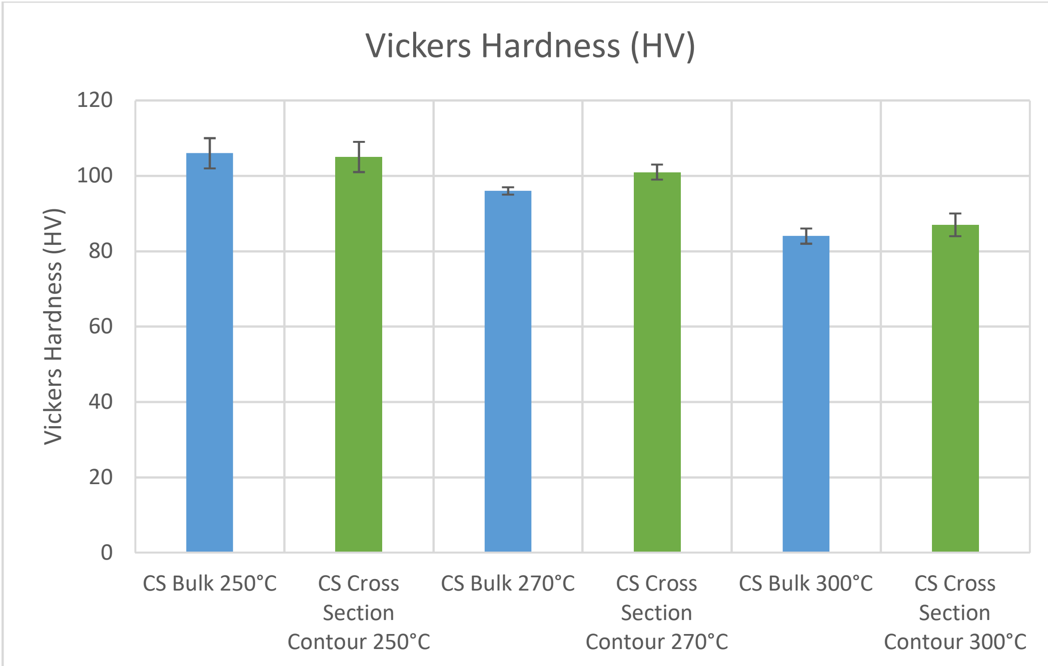

Figure 12 Vickers hardness results of the stress relief study completed on AM SLM CS samples

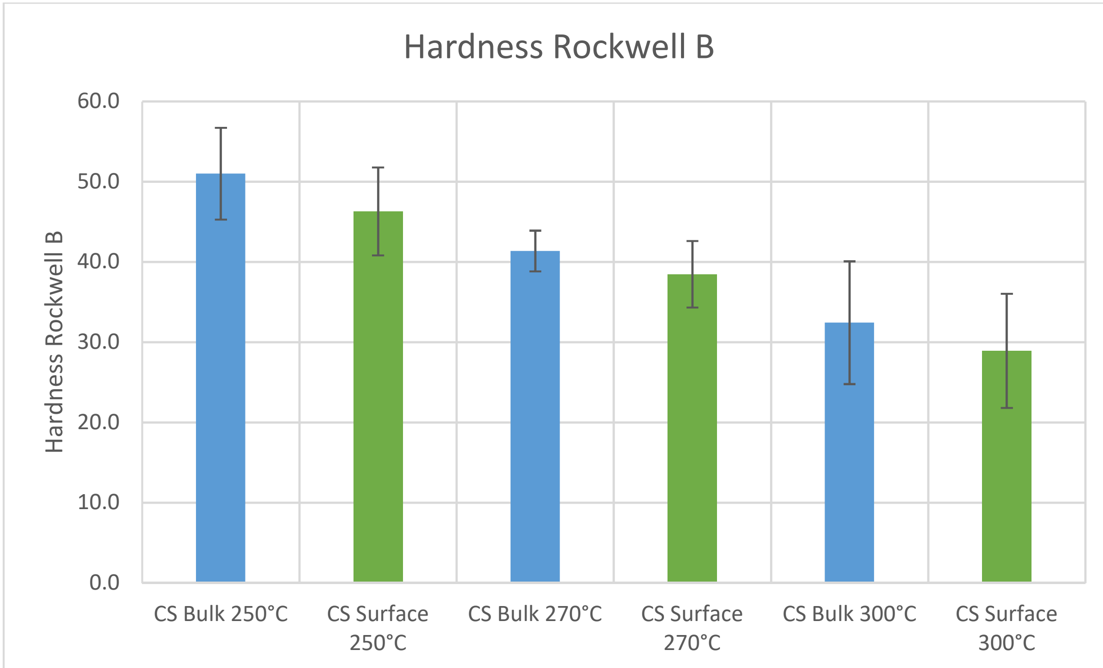

Figure 13 Rockwell B hardness results of stress relief study on AM SLM CS samples

6.3 Microstructure

6.3.1 Optical Microscopy

Optical microscopy was completed on the stress relieved AM SLM samples cross section contour edge to gain a better understanding of the melt pool geometries created from using different build parameters on the contour surface. The images can be observed in Figure 14 which indicate the melt pools, porosity, and partially melted powder particles on the surfaces.

The melt pool geometries for Conventional Slow and Conventional Fast, that have the same energy density, are similar in structure. Proprietary Low melt pools have a somewhat structured pattern along the cross section contour edge about 125 µm into the bulk from the contour surface and Proprietary High melt pools are completely structured approximately 500 µm following the cross section contour edge and stacked in the build direction. As the energy density increase the melt pools also increase because there is preheating of the sample from the previous layer and with each additional layer added more preheating occurs which increases the melt pools. This is seen on the edge of Proprietary Low in Figure 14 that is approximately 125 µm wide and on the edge of PH in Figure 14 that is approximately 500 µm wide. (White, 2014) The lower energy density samples, Figure 14 image a and b, have similar size and shape and have no unique melt pool characteristics concluding that if the ratio of power and velocity increases and the energy density stays the same the melt pool geometry will also stay the same.

The higher energy density the smoother the contour surface of the sample is. The optical images show particles on the contour surface of the samples called satellites. Satellites are solid metal powder particles that are connected to the melt pool on the surface of the as built part. These particles will increase the surface roughness of the samples. The higher the energy density the more heat that is concentrated on the metal powder which allow for fully melted powder along the contour surface. (Kurzynowski, 2012) Porosity can also be observed in the optical images.

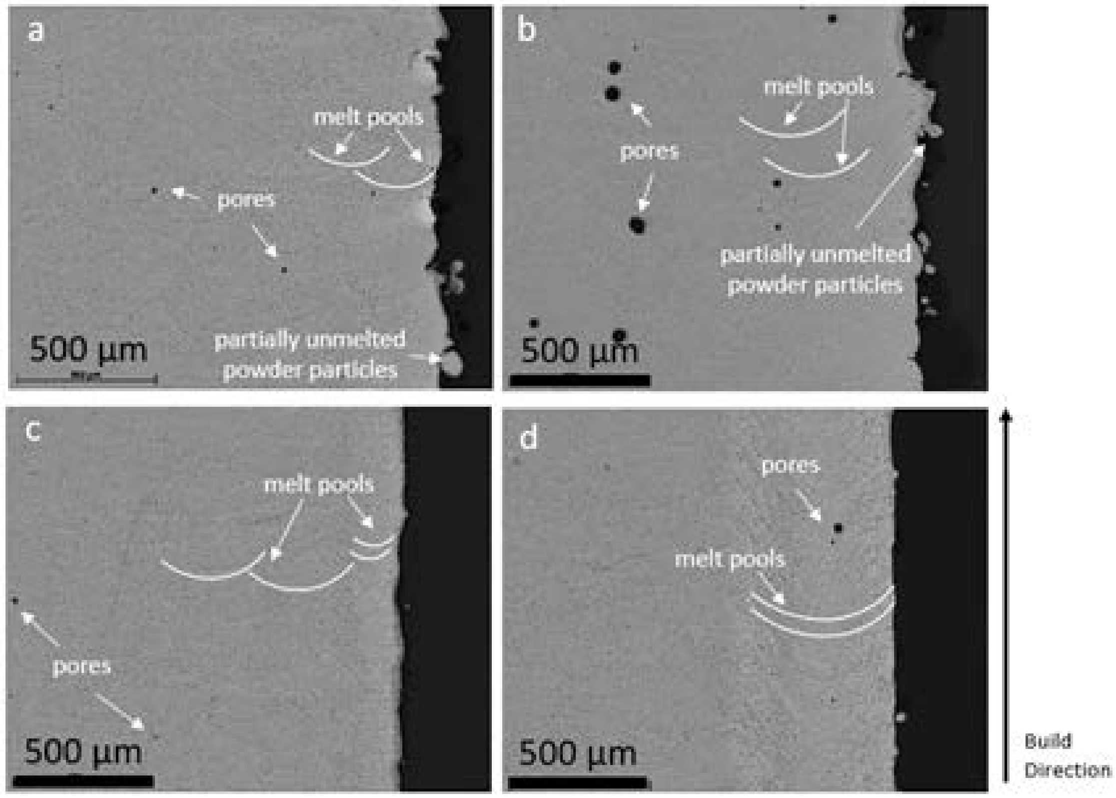

Figure 14 Optical images at 50x magnification of post stress relieved AM SLM samples cross section contour surface; a, b, and c) show similar melt pool geometries; a and b) unmelted powder particles can be observed; a – d) show pores present in the samples; a.) CS b.) CF c.) PL d.) PH

Optical microscopy was also completed on the surface finished AM SLM samples at the cross section contour edge. Images were taken to understand how the surface finished sample surfaces compare to the post stress relieved surface and to determine if the surface finishing step eliminated the contour melt pool surface differences between the samples. Optical images in Figure 15 for Conventional Slow, Conventional Fast, and Proprietary Low all show similar melt pool geometries on the surface finished samples. Proprietary High sample has a structured feature on the cross section contour surface which is approximately 150 µm from into the bulk from the contour of the sample which is seen in Figure 15 image d. This is the edge of the melt pool geometry of the post stress relieved sample not surface finished sample which can be observed in Figure 14 image d.

The contour surfaces in the images of Figure 15 are smooth because of the surface finishing technique completed on them. The surface roughness was decreased to 0.2 µm to 0.5 µm. Pores in the samples can be seen in the optical images.

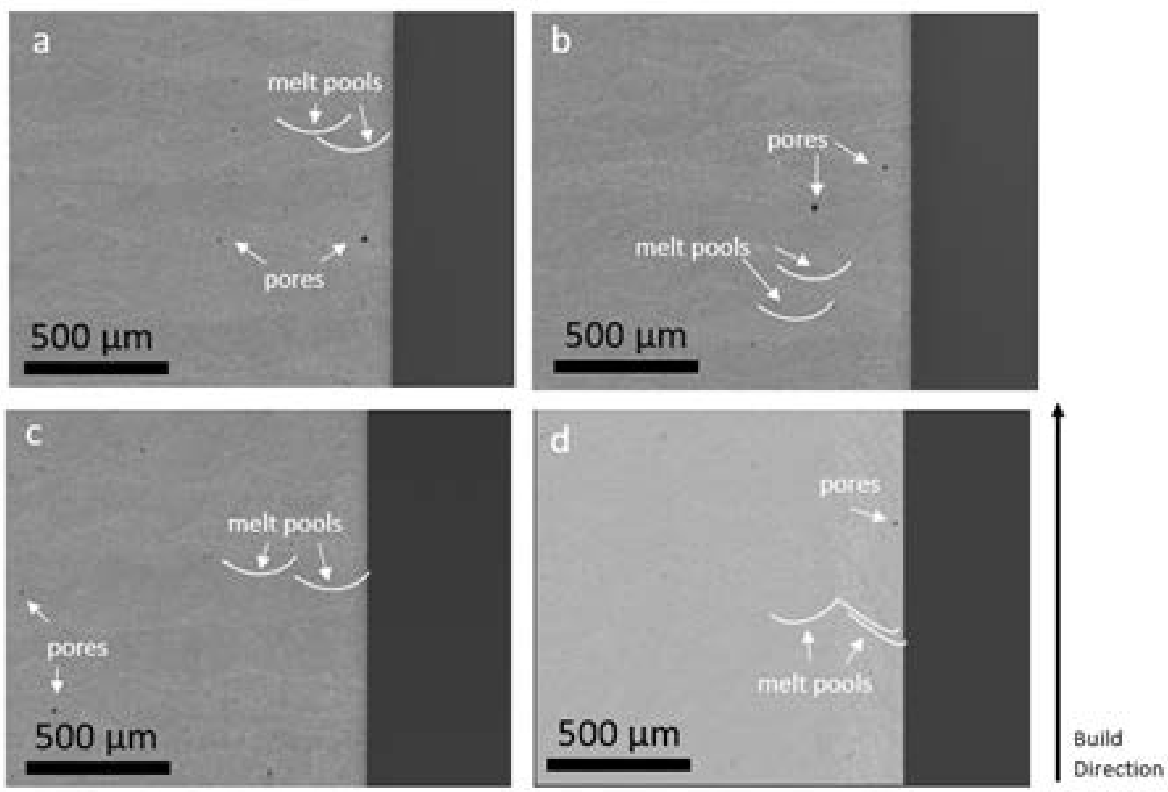

Figure 15 Optical images at 50x magnification of post stress relieved and surface finished AM SLM samples cross section contour surface; a, b, and c) show similar melt pool geometries; a – d) show pores present in the samples; a.) CS b.) CF c.) PL d.) PH

6.3.2 Electron Backscatter Diffraction

Electron backscatter diffraction (EBSD) was completed on the samples to understand differences in grain size and grain orientation. Figure 16 presents the AM SLM samples in the x direction, build direction of the part, along the cross section contour surface (located on the left side of the EBSD images) and the conventional aluminum alloys AA2618 and AA4032. Figure 17 presents the same samples as Figure 16 but in the z direction. Both images highlight the features that can be observed in the inverse pole figures such as melt pool boundaries, pores, and grain morphology.

Observed in the inverse pole figure (IPF) mapping of the AM SLM samples are areas with fine and equiaxed grains aligned in a curving shape which signifies the melt pool boundaries. Melt pool size and shape are driven by the build parameters and controlling the melt pools will allow for more lower resulting surface roughness. The higher the energy density the larger the melt pools will appear. This can be observed in the optical images in Figure 14. The low energy density samples melt pools have no unique features and appear the same in size and shape regardless of the power and velocity of the laser.

The fine and equiaxed grains that are observed along the melt pools are because this is where the cooling rate is slower when compared to the melt pool centers. This is due to the distribution of the laser. The higher the energy density as in the Proprietary High the finer and more equiaxed the grains appear this is because the melt pool geometries are structured, and the melt pool boundaries are close together unlike the other samples. The melt pool boundaries of the lower energy density samples have less equiaxed grains than high energy density samples because the sample experiences higher cooling rates which allows for longer columnar grains to form. (Iturrioz, 2018)

Conventional Slow, Figure 16 image a, near the contour surface imaged in the build direction, inverse pole figure mapping in the x-direction, have a columnar grain structure with the grains crystalographically aligned and the grain structure texturing is in the <001> direction with the columnar grains growing through the melt pool boundaries.

Conventional Fast, Figure 16 image b, imaged near the contour surface in the build direction, inverse pole figure mapping in the x-direction, the grains have a random crystallographic orientation, high misorientation of grains, that are a combination of columnar and equiaxed.

Proprietary Low, Figure 16 image c, on the cross section contour surface imaged in the build direction, inverse pole figure mapping in the x-direction, has a mixture of columnar grains that are crystalographically aligned with the texture in the <001> direction and grains with random crystallographic orientation.

Proprietary High, Figure 16 image d, near the contour surface imaged in the build direction, inverse pole figure mapping in the x-direction, grains show a random crystallographic orientation, high misorientation of grains, that are a combination of columnar and equiaxed in shape.

AA2618 and AA4032 EBSD images display that the grains are equiaxed and the morphology of the grain structure are similar however, AA2618 has a smaller grain size than AA4032. AA2618 images indicate there are iron containing constituents within the structure and AA4032 images indicate there are silicon containing constituents within the structure.

The differences that are observed in the microstructure is due to the temperature gradients that the samples experience. The elongated columnar grains are indicative of the thermal gradient direction. Therefore, the Conventional Slow has a thermal gradient that stays consistent between the build layers allowing for the formation of long columnar grains that are crystalographically aligned. Whereas the high energy density Proprietary High sample has columnar grains that are not as long, and the grains are not aligned in any direction but instead are fixed towards the center of the melt pools. (Iturrioz, 2018)

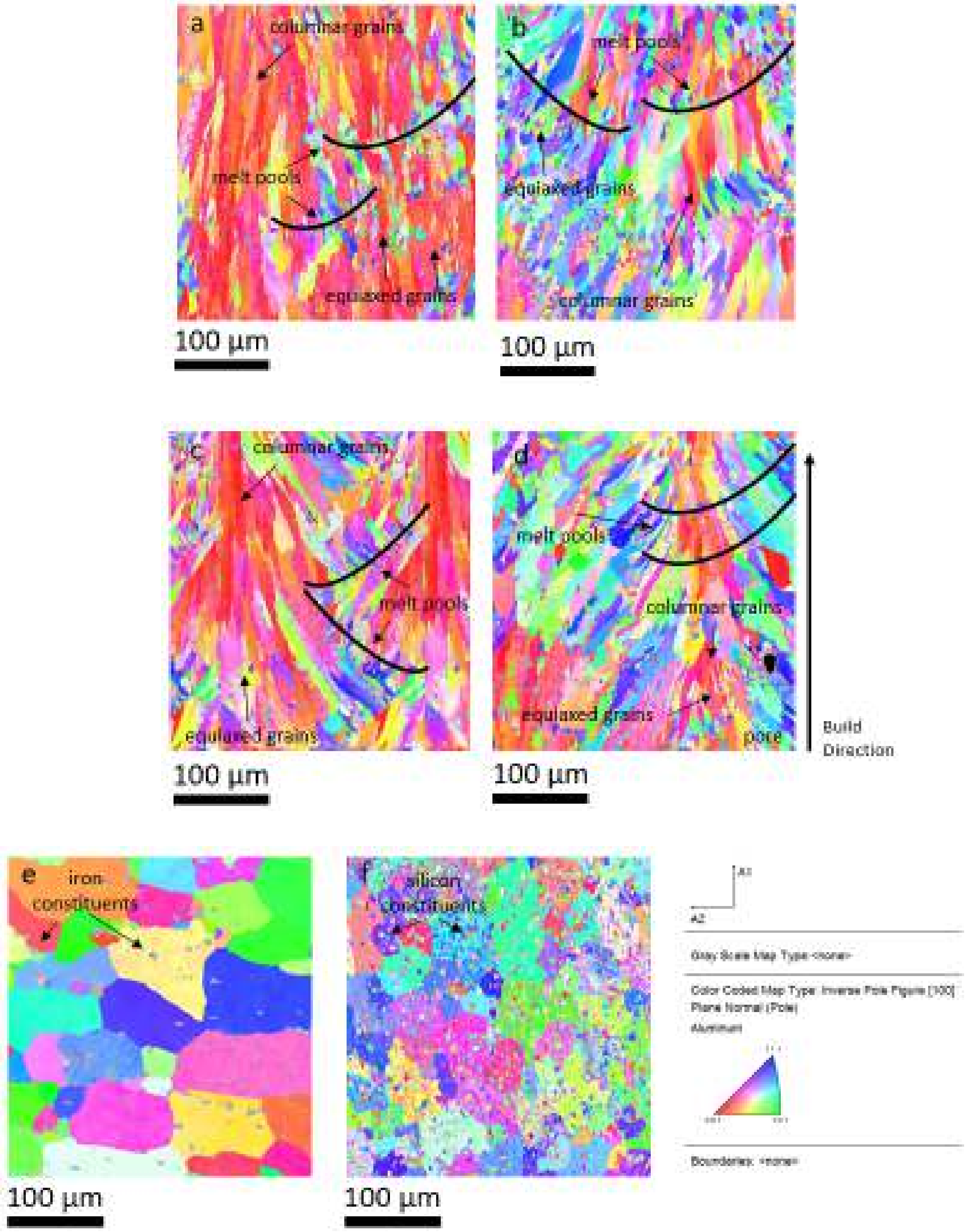

Figure 16 EBSD images (x-direction) of post stress relieved AM SLM samples cross section contour surface and conventional aluminum samples; a, b, and c) show similar melt pool geometries; a – d) columnar and equixed grains are observed; e and f) equiaxied grains are observed; e) shows iron constituents; f) shows silicon constituents; a.) CS b.) CF c.) PL d.) PH e.) AA2618 f.) AA4032

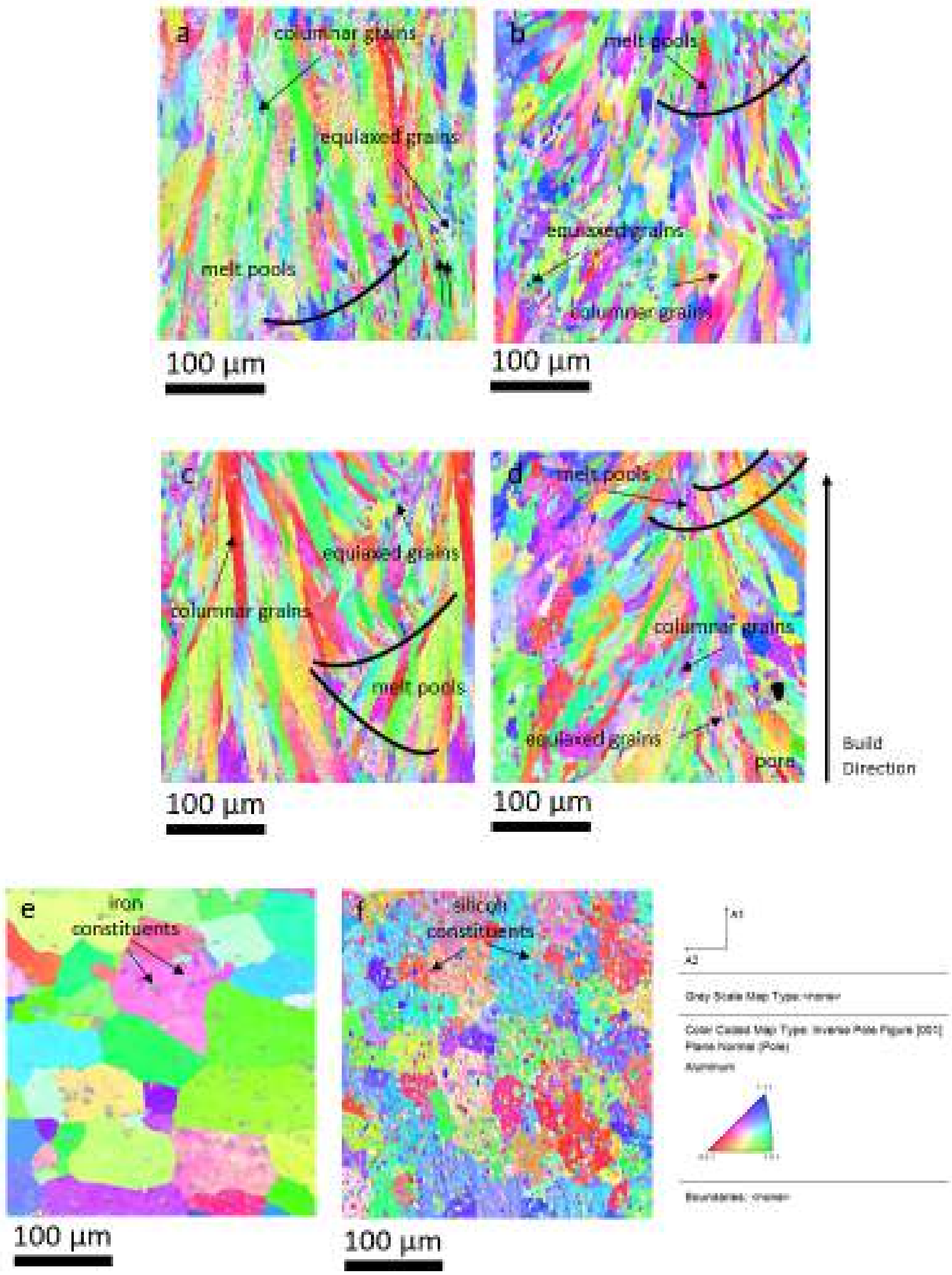

Figure 17 EBSD images (z-direction) of post stress relieved AM SLM samples cross section contour surface and conventional aluminum samples; a, b, and c) show similar melt pool geometries; a – d) columnar and equixed grains are observed; e and f) equiaxied grains are observed; e) shows iron constituents; f) shows silicon constituents; a.) CS b.) CF c.) PL d.) PH e.) AA2618 f.) AA4032

6.3.3 Scanning Electron Microscopy

Scanning electron microscopy images of the additive manufactured selective laser melted samples and the conventional aluminum samples can be seen in Figure 18. These images were taken near the cross section contour surface of the AM SLM samples and on the edge of AA2618 and AA4032.

Analysis shows the sub grain structure of the grains in the AM SLM samples, as evident in Figure 18 images a, b, c, and d. These subgrains have a similar fine equiaxed structure throughout the AM SLM samples. Proprietary High has more pores present than Conventional Slow and Proprietary Low and Conventional Fast has most pores present. Scanning electron microscopy-energy dispersive spectroscopy (SEM-EDS) was also completed to the samples. Conventional Slow, Conventional Fast, Proprietary Low, and Proprietary High analysis all report having aluminum, silicon, and magnesium as the main elements in the sample.

The AA2618 and AA4032 samples have large second phase constituents that overshadow the grain structure. The SEM images and SEM-EDS analysis for AA2618 show iron containing intermetallics in the matrix. The EBSD images also show the same iron containing intermetallics dispersed throughout the microstructure and they are similar in size between SEM and EBSD images. The intermetallics that are seen in the SEM images for AA2618 and AA4032 are Al_9FeNi. This is verified by the EDS measurement that showed levels of iron and nickel present.

The iron and nickel ratio is controlled at 1:1 for AA2618 to specifically form the Al_9FeNi intermetallic because it improves the resistance to plastic deformation. Copper was also observed in the EDS analysis which suggested the intermetallic phase Al_2CuMg is present which strengthens the AA4032. (Balducci, 2017, Novy, 2009)

SEM images and SEM-EDS analysis of AA4032 show silicon containing intermetallics within the matrix. The EBSD images for AA4032 also show the same silicon containing intermetallics which are approximately the same size in the SEM images and the EBSD images.

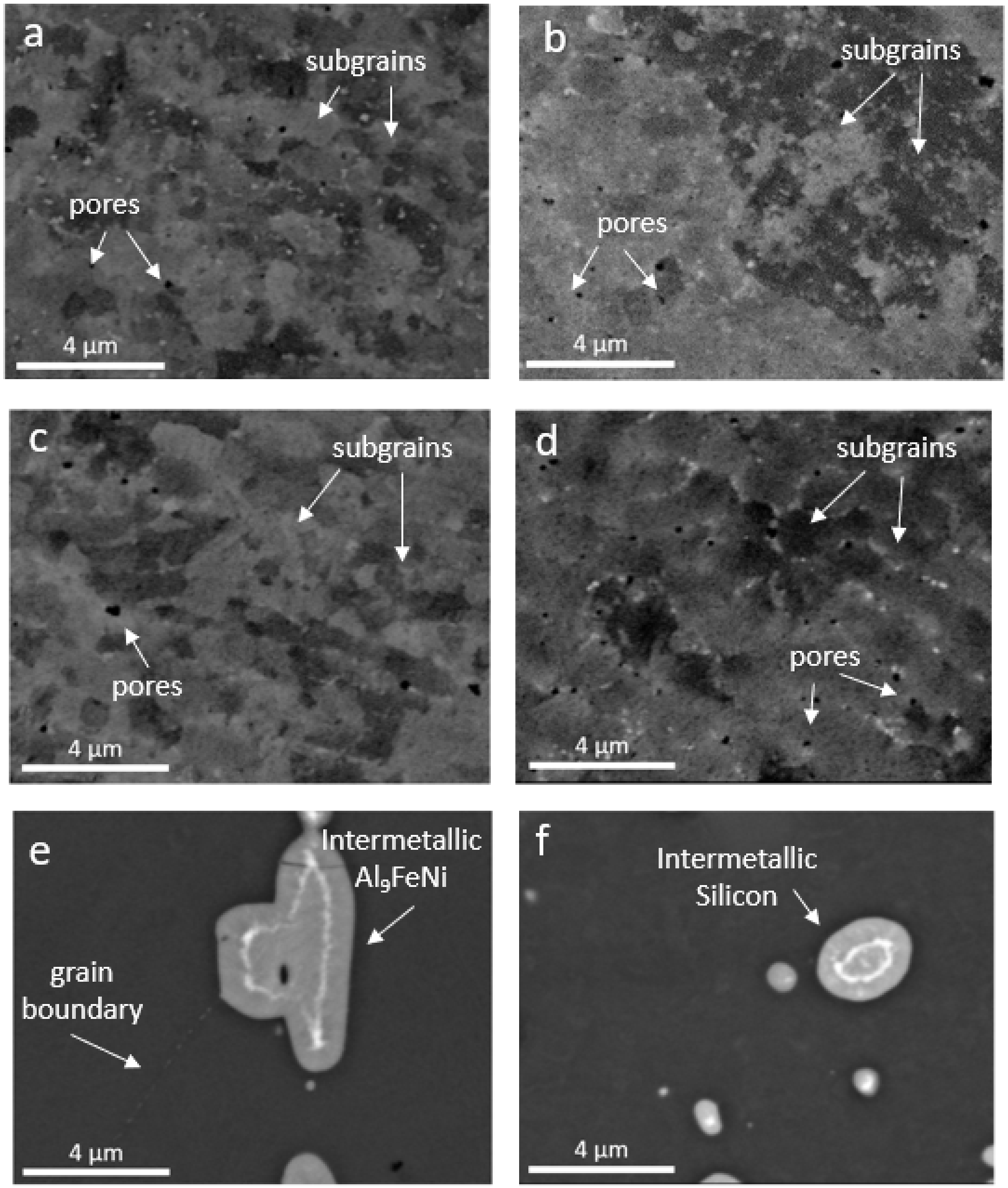

Figure 18 SEM backscattered images 10000x magnification of post stress relieved AM SLM samples cross section contour surface and conventional aluminum samples; a – d) show similar subgrain structure; e and f) intermetallic Al_9FeNi is observed; e) grain boundary is observed; a.) CS b.) CF c.) PL d.) PH e.) AA2618 f.) AA4032

6.4 Surface Properties

6.4.1 Contact Profilometry

In addition to the physical properties analysis, mechanical properties analysis, and microstructure analysis contact profilometry was completed to understand the surface roughness of the samples before the tribology testing. There is a difference in the surface roughness data that contact profilometry and non-contact optical topography measurements report. Contact profilometry is limited to a single trace with a diamond tip of 2 µm, therefore, depending on the topography of the sample the tip may not be able to capture the steep edges and deep valleys of the samples. This would cause the surface roughness to be lower than that of non-contact optical topography which has the ability to average many traces within the entire topography image. The surface roughness of contact profilometry was captured in both the transverse, perpendicular to the build direction, and longitudinal, parallel to the build direction, directions.

6.4.1.1 Post Stress Relieved AM Selective Laser Melted Contact Profilometry

Conventional Slow has an average roughness of 17.81 µm in the transverse direction which is significantly higher than Proprietary Low at 5.03 µm and Proprietary High at 5.05 µm in the transverse direction, which have increased energy density. Conventional Fast has a similar average roughness value to Conventional Slow at 18.76 µm in the transverse direction. The longitudinal direction and the transverse direction have similar roughness values because the sample topography is isotropic. The roughness values are located in Table 15.

This analysis demonstrates the ability to configure build parameters during the AM SLM printing process to optimize surface appearance and surface roughness parameters. The higher the energy density the lower the surface roughness parameters will be because the energy density changes the melt pool geometries because the cooling rate is slower. These melt pool geometries allow for fully melting metal powder particles together to form a smooth surface with no unmelted or partially melted powder particles attaching to the melt pool and remaining on the surface. Therefore, the low energy density of 0.47 J/mm^2 from the Conventional Slow and Conventional Fast is not optimized to be able to melt the metal powder particles with the laser power at the laser velocity and satellites are adhering to the contour surface. Satellites are solid metal powder particles that are connected to the melt pool on the surface of the as built part. (Kurzynowski, 2012)

Table 15 Contact profilometry of post stress relieved AM SLM samples

Sample	Surface	Average Ra-T_{avg} (µm)	Average Ra-L_{avg} (µm)
AlSi10Mg CS	Post Stress Relieved	17.8	17.6
AlSi10Mg CF	Post Stress Relieved	18.8	19.1
AlSi10Mg PL	Post Stress Relieved	5.0	4.9
AlSi10Mg PH	Post Stress Relieved	5.1	5.7

6.4.1.2 Surface Finished Samples Contact Profilometry

All the samples went through a surface finishing step aimed to reduce the surface roughness to below 0.5 µm. The surface finished condition of the samples have average values between 0.2

μm and 0.5 μm. The longitudinal direction and the transverse direction have similar roughness values. The contact profilometry values for the surface finished samples can be seen in Table 16.

Table 16 Contact profilometry of post stress relieved and surface finished AM SLM samples and conventional aluminum alloy samples

Sample	Surface	Average Ra-T_{avg} (μm)	Average Ra-L_{avg} (μm)
AlSi10Mg CS	Surface Finished	0.45	0.49
AlSi10Mg CF	Surface Finished	0.39	0.39
AlSi10Mg PL	Surface Finished	0.42	0.41
AlSi10Mg PH	Surface Finished	0.50	0.83
AA2618	Surface Finished	0.14	0.18
AA4032	Surface Finished	0.15	0.16

6.4.2 Non-Contact Optical Profilometry

Non-contact optical profilometry was completed on the post stress relieved additive manufactured selective laser melted samples and the surface finished samples in the transverse direction, perpendicular to the build direction and the longitudinal direction, parallel to the build direction.

6.4.2.1 Post Stress Relieved AM Selective Laser Melted Non-Contact Optical Profilometry

The post stress relieved AM SLM samples non-contact optical profilometry measurements show that Conventional Slow and Conventional Fast, which have the same energy density have a similar surface roughness. AM SLM sample topography images can be seen in Figure 19. Proprietary Low and Proprietary High which have a higher energy density, have significantly lower surface roughness. The surface roughness of the post stress relieved AM SLM samples have similar roughness values in the transverse and longitudinal directions because the sample topography is isotropic in nature. The non-contact optical profilometry roughness values in the transverse direction for Conventional Slow was 26.1 µm, Proprietary Low was 5.4 µm, Proprietary High was 4.8 µm, and Conventional Fast was 30.8 µm. Table 17 portrays the non-contact optical profilometry roughness parameters for the AM SLM samples in the post stress relieved condition. The differences observed in the contact profilometry and the non-contact optical profilometry results are because of the limitations of the contact profilometry. The limitations are based on the size of the diamond tip which has difficulty measuring the steep curves and edges observed on the surface of the some of the post stress relieved AM SLM samples.

This analysis demonstrates the ability to configure build parameters during the AM SLM printing process to optimize surface appearance and surface roughness parameters. The higher the energy density the lower the surface roughness parameters will be because the energy density changes the melt pool geometries because of the slow cooling rate. The differences in the melt pool geometries allow for the powder particles to fully melt together and form a smooth surface with no unmelted or partially melted powder particles remaining on the surface, called satellites. Whereas with the Conventional Slow and Conventional Fast the energy density is low at 0.47 J/mm^2. These power and velocity combinations are not optimized to be able to melt the metal powder particles at the laser velocity created satellites on the contour surface which are partially melted powder particles.

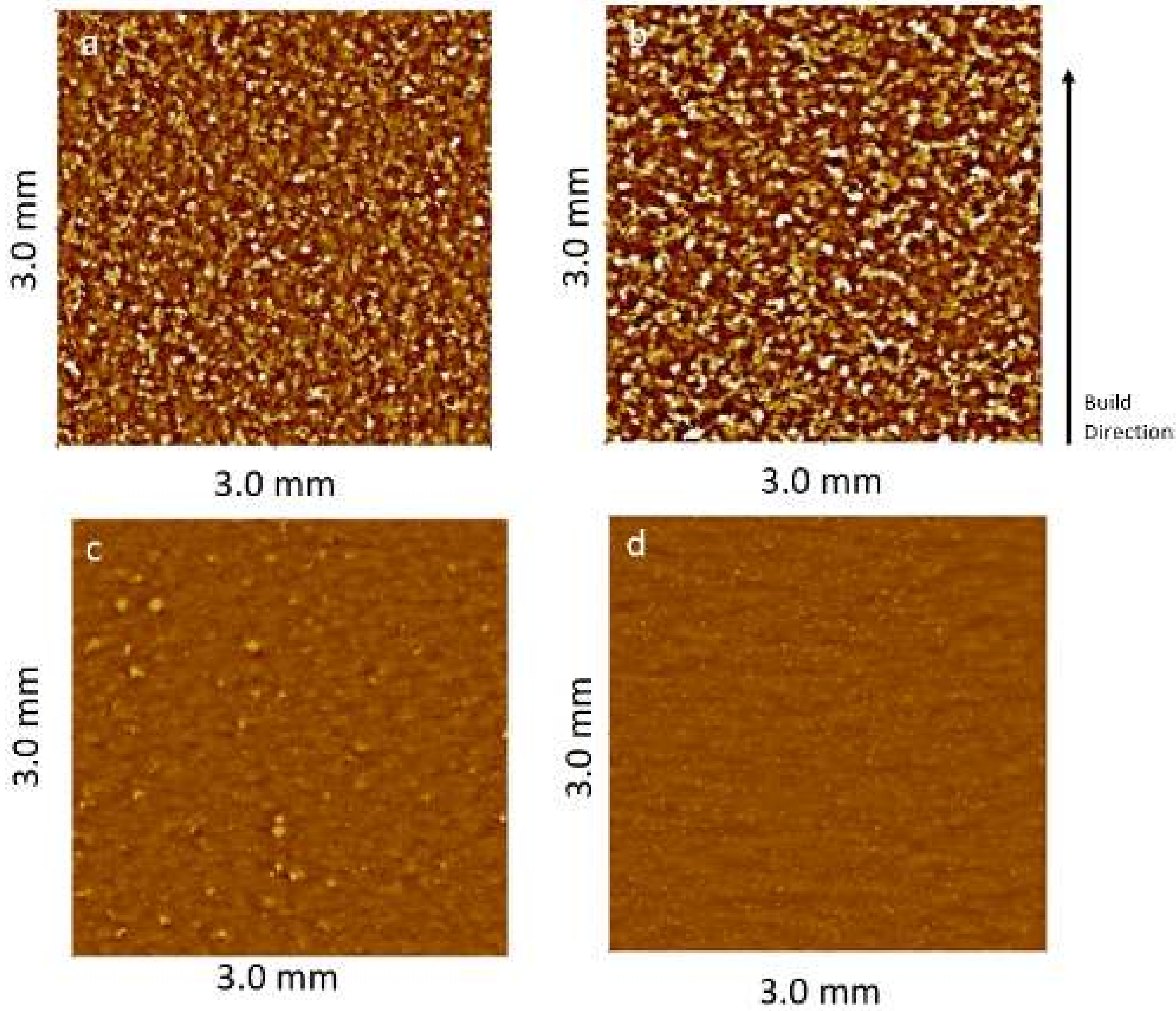

Figure 19 Topography images of post stress relieved AM SLM samples (color scale ± 100 µm) a.) CS b.) CF c.) PL d.) PH

Table 17 Non-contact optical profilometry of post stress relieved AM SLM samples

Sample	Surface	Average Ra-T_{avg} (µm)	Average Ra-L_{avg} (µm)	Average Sa (µm)
AlSi10Mg CS	Post Stress Relieved	26.1	26.0	25.3
AlSi10Mg CF	Post Stress Relieved	30.8	31.0	31.3
AlSi10Mg PL	Post Stress Relieved	5.4	5.4	5.4
AlSi10Mg PH	Post Stress Relieved	4.8	4.8	4.8

The Conventional Slow image appears to have unmelted powder particles on the surface causing the increase in roughness values. Figure 20 shows a zoom box of the Conventional Slow non-contact optical profilometry images. The zoomed image shows partially melted powder particles on the surface. A cross sectional analysis was completed on these particles to determine the diameter and the values measured were between 30 µm to 170 µm. These values correlate with the powder particle distribution for the two powders that is shown in Figure 3. This confirms that the low energy density parameters are not optimized for creating smooth surfaces.

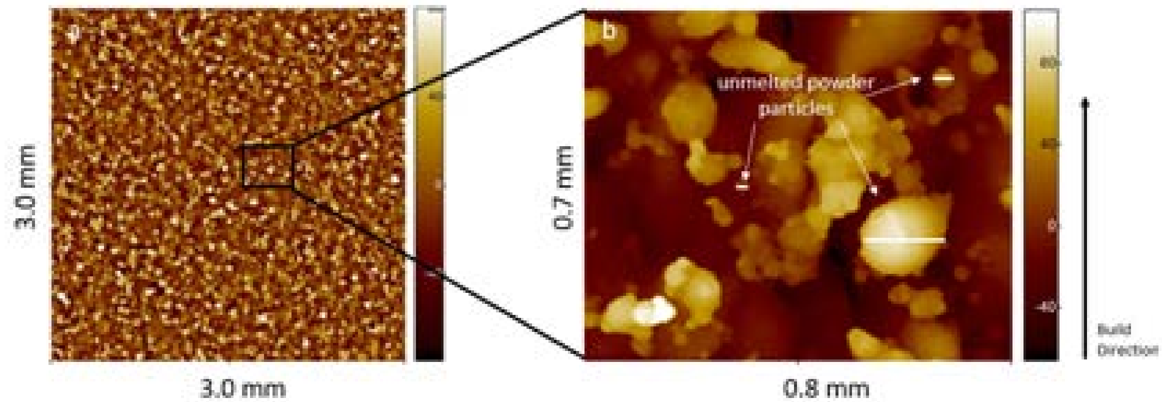

Figure 20 Topography image of Conventional Slow AM SLM sample a.) CS b.) zoom box of a. shows unmelted powder particles on the contour surface

6.4.2.2 Surface Finished Samples Non-Contact Optical Profilometry

Surface finished samples were mechanically polished to normalize the roughness across all the samples. The average roughness is between 0.12 and 0.39 µm for all the samples. The topography images of all of the surface finish samples can be observed in Figure 21 and the roughness values are portrayed in Table 18. The directional topography observed in the images are the polishing marks from the surface finishing step. Field of view for the images is 3.0 mm x 1.8 mm and the images are filtered with L_c 0.8 mm and L_s 2.5 µm filters.

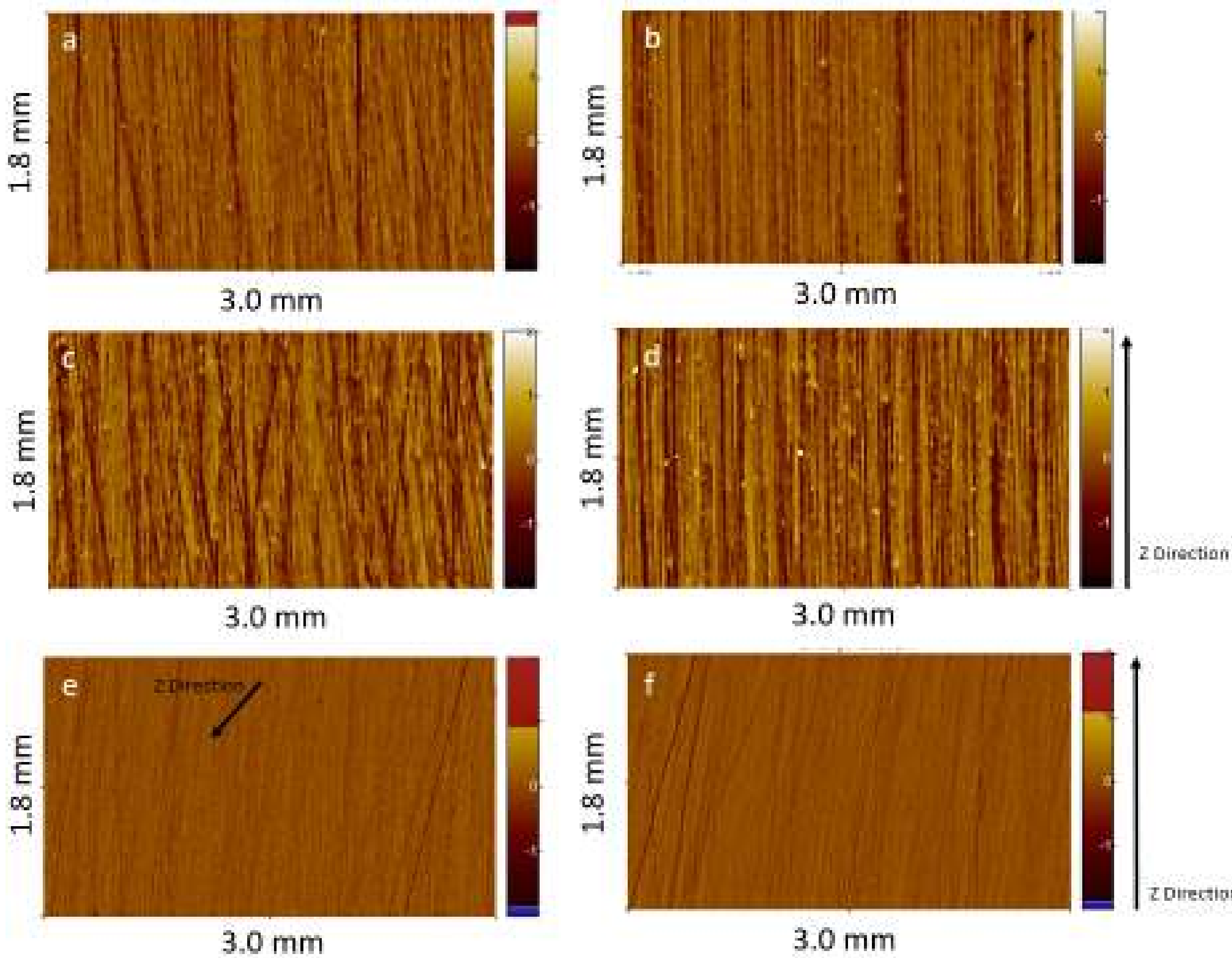

Figure 21 Topography images of post stress relieved and surface finished AM SLM samples and conventional aluminum samples (color scale ± 2 µm) a.) CS b.) CF c.) PL d.) PH e.) AA2618 f.) AA4032

Table 18 Non-contact optical profilometry of post stress relieved and surface finished AM SLM samples and conventional aluminum alloy samples

Sample	Surface	Average Ra-T_{avg} (μm)	Average Ra-L_{avg} (μm)	Average Sa (μm)
AlSi10Mg CS	Surface Finished	0.36	0.30	0.36
AlSi10Mg CF	Surface Finished	0.36	0.25	0.36
AlSi10Mg PL	Surface Finished	0.32	0.25	0.32
AlSi10Mg PH	Surface Finished	0.33	0.27	0.33
AA2618	Surface Finished	0.16	0.13	0.16
AA4032	Surface Finished	0.17	0.15	0.17

6.5 Reciprocating Tribology Experiment

6.5.1 Post Stress Relieved AM Selective Laser Melted Samples Tribology Experiment

The tribology wear testing was completed on the post stress relieved samples, which consisted of four additive manufactured selective laser melted samples with varying build parameters.

The wear scar depth was measured after 5 minutes, 10 minutes, 20 minutes, and 40 minutes for a total sliding distance of 9 m, 18 m, 36 m, and 72 m respectively by a non-contact optical profilometer. Samples were not removed from the set up to take the images, the instrumentation allows for full stage movement to position the sample under the non-contact optical instrument, to capture the images.

Topography images of the wear scars for the AM SLM samples can be seen in Figure 22. Non-contact surface analysis was used to determine the wear rate of the as received tribology experiment samples by measuring the depth of the wear scar across the entire image. The wear depth for the samples throughout the tribology wear test can be seen in Table 19. The wear volume was calculated from the wear depth which can be seen in Table 20 using equation 5-3 and the wear rate was calculated according to the Archard equation, 5-4, and the wear rate data is portrayed in Table 21. Figure 23 illustrates the calculated wear rates based on the Archard equation throughout the tribological testing.

The wear rates show that Proprietary High has the lowest calculated wear rate followed by Conventional Slow, Proprietary Low, and then Conventional Fast. The wear scar depths differ from each other with Conventional Slow and Proprietary High having approximately the same wear scar depth which is less than the Proprietary Low and Conventional Fast AM SLM samples.

A more thorough examination of the tribology results will be discussed in the next chapter.

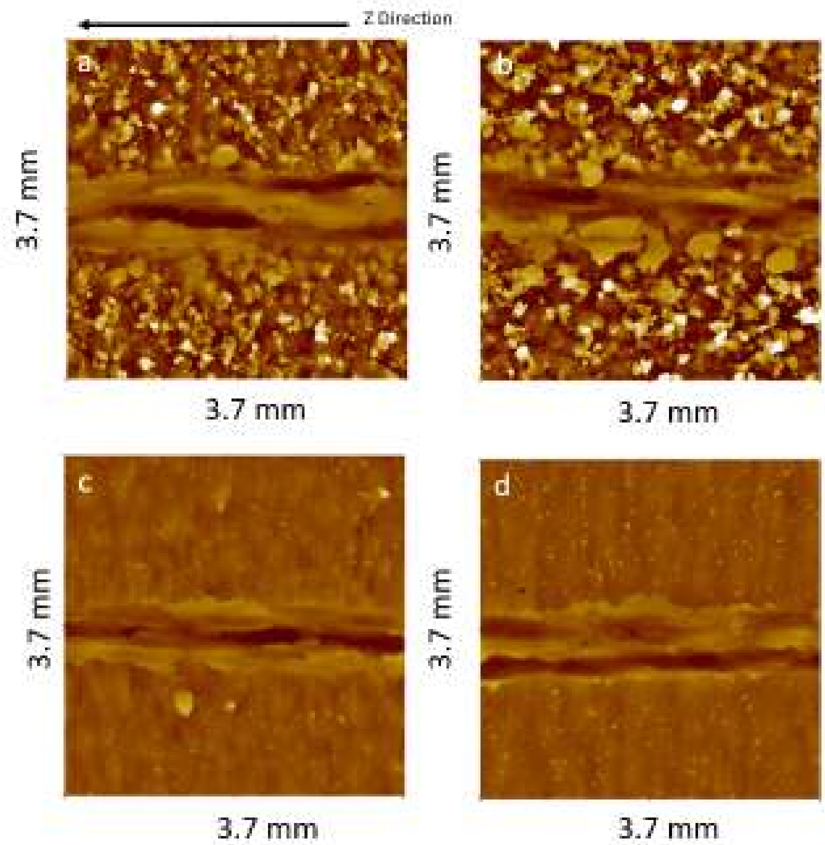

Figure 22 Non-contact optical profilometry images of wear scars of post stress relieved AM SLM samples at 72 meter distance (color scale ± 100 µm) a.) CS b.) CF c.) PL d.) PH

Table 19 Tribological testing wear scar depth measurement of post stress relieved AM SLM samples

Sample	Surface	9 m Distance Wear Scar Depth (μm)	18 m Distance Wear Scar Depth (μm)	36 m Distance Wear Scar Depth (μm)	72 m Distance Wear Scar Depth (μm)
CS Average	Post Stress Relieved	19.68	35.31	50.10	62.93
CF Average	Post Stress Relieved	36.91	51.83	69.53	81.02
PL Average	Post Stress Relieved	26.06	47.45	66.63	76.00
PH Average	Post Stress Relieved	14.86	26.69	52.89	51.73

Table 20 Tribological testing wear volume measurement of post stress relieved AM SLM samples

Sample	Surface	9 m Distance Wear Scar Volume (mm^3)	18 m Distance Wear Scar Volume (mm^3)	36 m Distance Wear Scar Volume (mm^3)	72 m Distance Wear Scar Volume (mm^3)
CS Average	Post Stress Relieved	0.014503	0.024301	0.068537	0.015555
CF Average	Post Stress Relieved	0.038516	0.065987	0.089055	0.099451
PL Average	Post Stress Relieved	0.046476	0.069059	0.098222	0.078298
PH Average	Post Stress Relieved	0.028353	0.028980	0.033579	0.035938

Table 21 Tribological testing wear rate of post stress relieved AM SLM samples calculated from the Archard equation

Sample	Surface	9 m Distance Wear Rate (mm^3/Nm)	18 m Distance Wear Rate (mm^3/Nm)	36 m Distance Wear Rate (mm^3/Nm)	72 m Distance Wear Rate (mm^3/Nm)
CS Average	Post Stress Relieved	0.005847	0.019254	0.039456	0.062576
CF Average	Post Stress Relieved	0.020881	0.040736	0.075822	0.107070
PL Average	Post Stress Relieved	0.012852	0.034833	0.067329	0.087128
PH Average	Post Stress Relieved	0.004148	0.012057	0.047764	0.045940

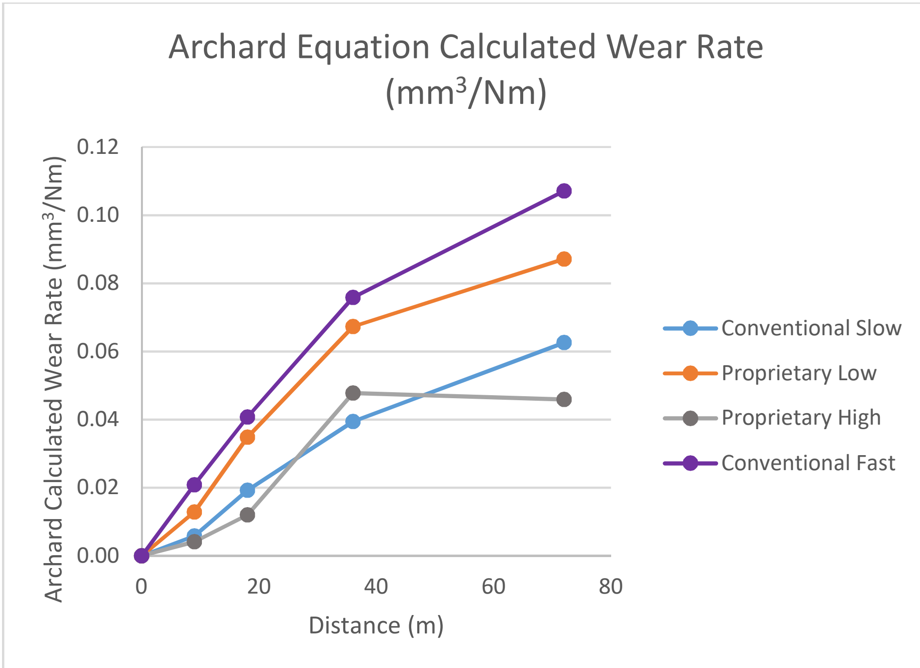

Figure 23 Tribological testing wear rate of post stress relieved AM SLM samples calculated from the Archard equation

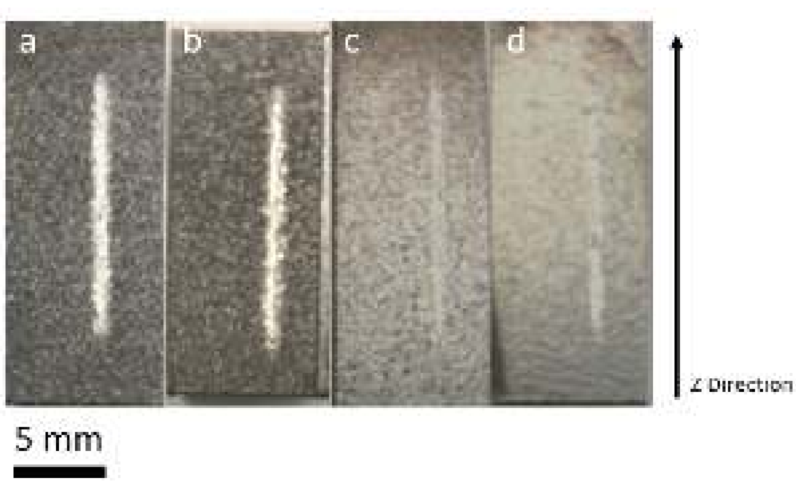

Figure 24 Wear scars of post stress relieved AM SLM samples at 72 meter distance a.) CS b.) CF c.) PL d.) PH

6.5.2 Surface Finished Samples Tribology Experiment

The tribology wear testing was completed on the surface finished samples, which consisted of AM SLM AlSi10Mg samples and conventionally made aluminum samples that were surface finished to have similar roughness parameters which calculated to be between 0.2 μm and 0.5 μm

The wear scar depth was measured after 5 minutes, 10 minutes, 20 minutes, and 40 minutes for sliding distances of 9 m, 18 m, 36 m, and 72 m respectively. The wear scar depths are significantly different from each other. The wear depth for the samples throughout the tribology wear test can be seen in Table 22. Non-contact surface analysis demonstrates the differences in the wear scar. The analysis also shows the conventional AA2618 and AA4032 have the lowest wear rate and Proprietary High AM SLM samples exhibiting the lowest wear rate of the AM SLM samples, following by Conventional Slow, Proprietary Low, and then Conventional Fast.

The wear scars of the additive manufactured selective laser melted samples Conventional Slow, Conventional Fast, and Proprietary Low appear to be coarser than Proprietary High, AA2618, and AA4032 with material displacement on the sides of the wear scars which can be observed in Figure 25 images a, b, and c.

The wear rate was calculated according to the Archard equation, 5-4, by way of the wear volume which was calculated based on equation 5-3. These values are reported in Table 23. The wear rates show that the conventional AA2618 and AA4032 materials had the lowest calculated wear rate with Proprietary High being slightly above AA4032 following closely by Conventional Slow. The wear rate can be seen in Table 24 and is illustrated in Figure 26 for the surface finished samples.

A more thorough examination of the tribology results will be discussed in the next chapter.

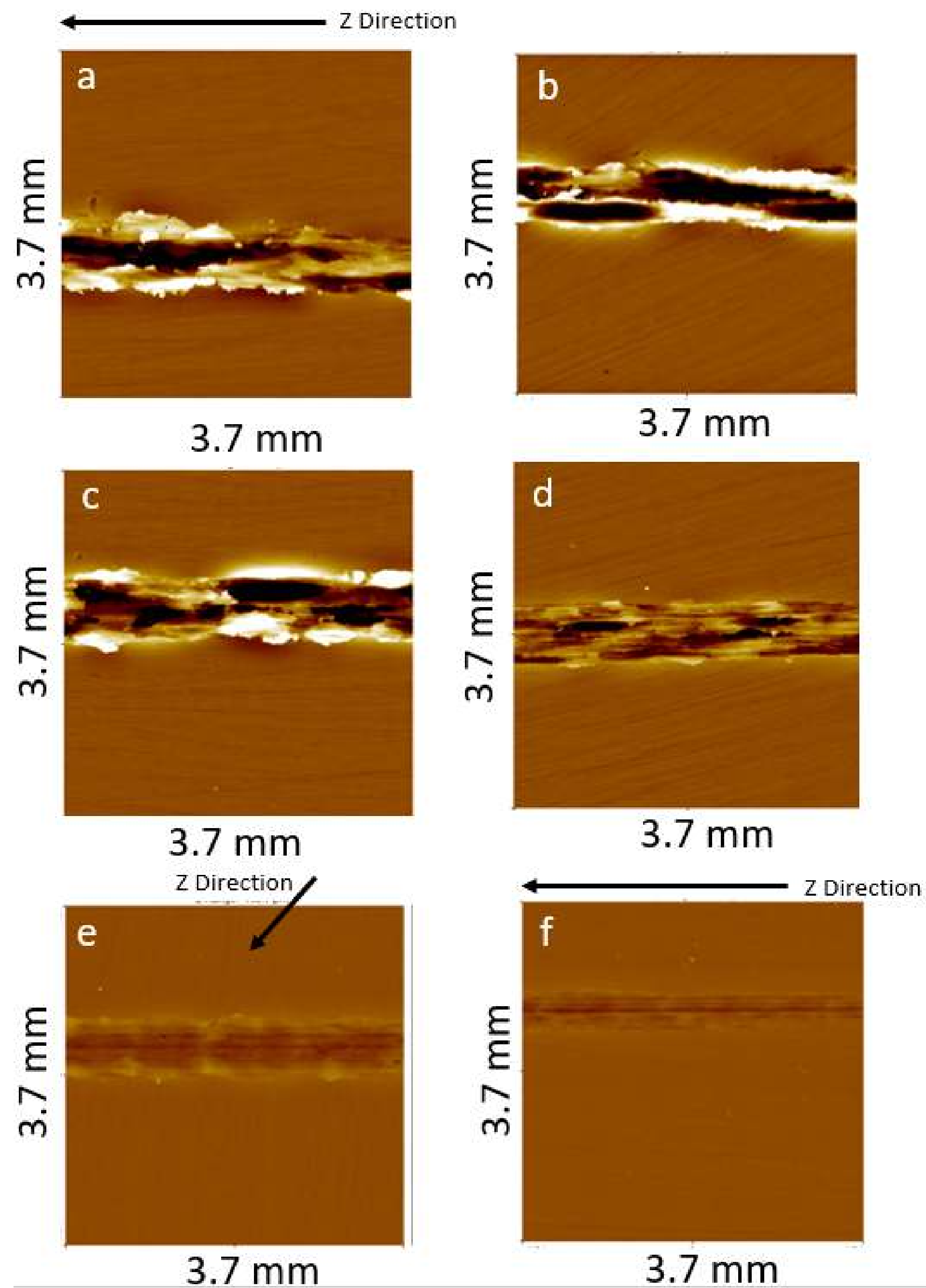

Figure 25 Non-contact optical profilometry images of wear scars of post stress relieved and surface finished AM SLM samples at 72 meter distance (color scale ± 20 µm) a.) CS b.) CF c.) PL d.) PH and conventional aluminum alloys e.) AA2618 f.) AA4032

Table 22 Tribological testing wear scar depth measurement of post stress relieved and surface finished AM SLM samples and conventional aluminum samples

Sample	Surface	9 m Distance Wear Scar Depth (μm)	18 m Distance Wear Scar Depth (μm)	36 m Distance Wear Scar Depth (μm)	72 m Distance Wear Scar Depth (μm)
CS Average	Surface Finished	30.26	40.31	61.24	32.32
CF Average	Surface Finished	47.57	66.47	76.93	81.61
PL Average	Surface Finished	50.47	62.01	80.36	66.52
PH Average	Surface Finished	37.03	39.52	41.00	42.89
AA2618 Average	Surface Finished	8.97	12.07	11.20	13.13
AA4032 Average	Surface Finished	7.49	8.03	8.85	10.57

Table 23 Tribological testing wear volume of post stress relieved and surface finished AM SLM samples and conventional aluminum samples

Sample	Surface	9 m Distance Wear Scar Volume (mm^3)	18 m Distance Wear Scar Volume (mm^3)	36 m Distance Wear Scar Volume (mm^3)	72 m Distance Wear Scar Volume (mm^3)
CS Average	Surface Finished	0.000161	0.000135	0.000190	0.000022
CF Average	Surface Finished	0.000428	0.000367	0.000247	0.000138
PL Average	Surface Finished	0.000516	0.000384	0.000273	0.000109
PH Average	Surface Finished	0.000315	0.000161	0.000093	0.000050
AA2618 Average	Surface Finished	0.000014	0.000013	0.000005	0.000003
AA4032 Average	Surface Finished	0.000010	0.000006	0.000004	0.000002

Table 24 Tribological testing wear rate of post stress relieved and surface finished AM SLM samples and conventional aluminum samples calculated from the Archard equation

Sample	Surface	9 m Distance Wear Rate (mm^3/Nm)	18 m Distance Wear Rate (mm^3/Nm)	36 m Distance Wear Rate (mm^3/Nm)	72 m Distance Wear Rate (mm^3/Nm)
CS Average	Surface Finished	0.000161	0.000135	0.000190	0.000022
CF Average	Surface Finished	0.000428	0.000367	0.000247	0.000138
PL Average	Surface Finished	0.000516	0.000384	0.000273	0.000109
PH Average	Surface Finished	0.000315	0.000161	0.000093	0.000050
AA2618 Average	Surface Finished	0.000014	0.000013	0.000005	0.000003
AA4032 Average	Surface Finished	0.000010	0.000006	0.000004	0.000002

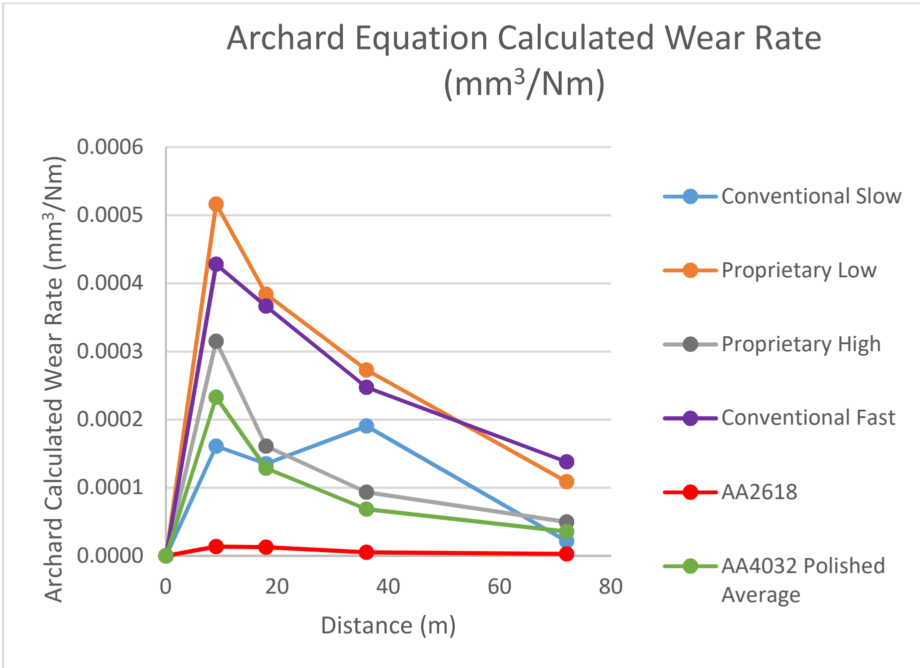

Figure 26 Tribological testing wear rate of post stress relieved and surface finished AM SLM samples and conventional aluminum samples calculated from the Archard equation

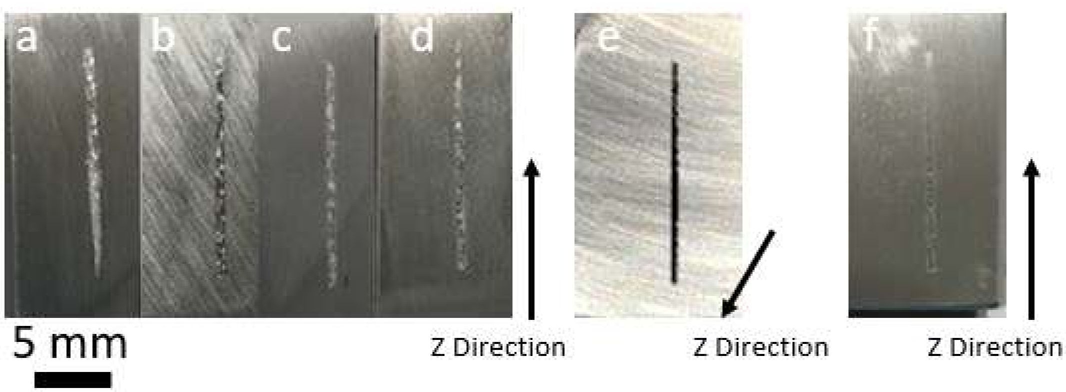

Figure 27 Wear scars of post stress relieved and surface finished AM SLM samples a.) CS b.) CF c.) PL d.) PH and conventional aluminum alloys e.) AA2618 f.) AA4032

7.0 Summary and Conclusions

The additive manufacturing selective laser melting process produces material properties that differ from conventionally made parts. This research investigated the material properties of the AM SLM parts including composition, mechanical properties, microstructure, and wear performance. The implications of this research are to better understand how AM SLM build parameters affect the mechanical and tribological performance of aluminum alloys and how this can be leveraged to optimize performance beyond that of conventionally manufactured parts.

The AM SLM samples were built using four different parameter sets which can be seen in detail in Table 7. Conventional Slow and Conventional Fast had the same energy density, however, Conventional Fast had power and velocity increased at the same ratio. Proprietary Low build parameters had increased the energy density from Conventional Slow and Proprietary High build parameters increased energy density even more. These parameters were chosen to create differences in the microstructure and mechanical properties.

The wear mechanics testing consisted of two parts: part one is to understand the wear mechanics of the post stress relieved AM SLM samples with no surface finishing and part two is to understand the wear mechanics of the AM SLM samples and the conventional AA2618 and AA4032 samples that have been surface finished to the same roughness. Surface finishing was completed on the samples to be able to gain an understanding of how the physical and mechanical properties can impact the wear mechanics while removing surface roughness as a factor. The surface finishing step was similar to that of a polishing procedure with a target roughness between 0.2 µm and 0.5 µm by varying abrasive sand paper to normalize the roughness of the samples. The amount of material that was removed from the samples during the surface finishing polishing procedure was approximately 250 µm to 350 µm.

7.1 Wear Mechanics of Post Stress Relieved AM SLM Samples

Tribological testing was completed on the post stress relieved AM SLM samples. The wear scars as seen by the topography images in Figure 22 are similar with no pile up on the sides of the wear scar. The wear depth was between 50 µm and 80 µm deep calculated from the topography images and in turn the wear volume and then the wear rate were calculated. The wear rate of the samples shows that Conventional Slow and Proprietary High samples had the lowest calculated wear rate with Proprietary Low and Conventional Fast following. Since the hardness values are all the same because of the stress relief process that normalized them the main impacts to the wear rate are from surface roughness and microstructure. The calculated wear rate for the AM SLM post stress relieved samples are all still increasing therefore the testing should be continued past the 72 m to understand the full wear mechanics of the post stress relieved AM SLM samples.

The microstructures of Conventional Slow and Proprietary High will be discussed first since these samples had the lowest calculated wear rate moving to the Proprietary Low and then Conventional Fast. The microstructure of the AM SLM post stress relieved samples are all different which is directly related to the build parameters used to produce the parts.

Conventional Slow build parameters are 80 W for power and 900 mm/s for velocity, which calculates to a low energy density of 0.47 J/mm^2. These parameters allow for a high cooling rate compared to the other calculated energy densities. The parameters directly affect the melt pool boundaries and as seen in Figure 14a, the melt pool boundaries have no specific structure associated with them. In the EBSD analysis it was shown that the melt pool boundaries also produce fine equiaxed grains which is because there is higher cooling rate that is experienced at the melt pool boundaries compared to the melt pool centers. The EBSD analysis also illustrates that the Conventional Slow build parameters produce long columnar grains that are oriented in the <001> direction.

The low energy density also affects the surface roughness of the samples. The low laser power does not create enough heat to be able to completely melt the powder particles along the surface which causes satellites to form. These satellites are unmelted powder particles that attach to the contour surface and create high surface roughness. They can also become third body wear particles during the tribological wear. The surface roughness of the different post stress relieved AM SLM samples was measured which showed that the low energy density samples had significantly higher surface roughness parameters compared to the higher energy density samples. Conventional Slow has a low calculated energy density therefore a high surface roughness that was measured at 26.0 µm by non-contact optical profilometry.

The Rockwell B hardness values for Conventional Slow were slightly higher than the Conventional Fast and the Proprietary low which would impact the wear rate by lowering it.

Proprietary High samples had the highest calculated energy density. The microstructure of this samples was significantly different than the Conventional Slow microstructure. The high energy density produced melt pool geometries that were approximately 500 µm wide. These melt pool boundaries also had more equiaxed grains that can be observed in the EBSD images in Figure 16d. The sample also had columnar grains that had a crystallographic random orientation and also followed the shape of the melt pools with the grains pointing to the center of the melt pools. The energy density of this material is high which suggests lower cooling rate of the material because of the concentration of the laser during the build process. Which is the reason the melt pool geometries are larger than what is observed in the other AM SLM samples. Since this material seems to have finer grain structure when compared to the other AM SLM samples this would suggest the material would have higher hardness properties. However, as stated above the stress relief temperature had normalized the hardness values of the AM SLM samples.

The high energy density of Proprietary High allows for complete melting of the powder particles and no satellites can form on the surface. The surface roughness of this sample as measured by non-contact optical profilometry and it is the lowest of the AM SLM samples at 4.8 μm.

The Rockwell hardness B values for Proprietary High also tested to be the highest compared with the other AM SLM post stress relieved samples. This reinforces the Hall Petch equation which states the smaller the grain size the higher the hardness. This slightly higher tested hardness would factor into the lower calculated wear rate.

The sample with the next lowest wear rate of the post stress relieved AM SLM samples is the Proprietary Low sample. This sample has a calculated energy density that is increased from the Conventional Slow but is lower than the Proprietary High energy density. The microstructure of this sample is a mixture of the Conventional Slow and the Proprietary High. It has long columnar grains that are partially oriented in the <001> direction and are also have a random crystalographically orientation as observed in the EBSD images. The EBSD images also show small equiaxed grains that are indicative of the melt pool boundaries. The melt pool boundaries on this samples are similar to Conventional Slow where there is no structure seen in most of the image except for against the contour edge for approximately 125 μm into the bulk. This structuring is small melt pools that are stacked on top of one another similar to that of Proprietary High. The energy density drives this melt pool geometry behavior by having a slow cooling rate.

The higher energy density that is associated with Proprietary Low also allows for limited satellites to form on the surface. These few satellite particles increase the surface roughness slightly, but the overall surface roughness is significantly lower than the Conventional Slow and Conventional Fast at 5.4 μm measured by non-contact optical profilometry.

As stated, the Conventional Fast sample was printed with build parameters of 210 W for power and 2360 mm/s for velocity and a calculated energy density the same as Conventional Slow at 0.47 J/mm^2. These build parameters give the Conventional Fast samples a unique microstructure. The microstructure is made up of columnar grains that have a random crystallographic orientation. These grains also tend to structure themselves according to the melt pool geometry with the grains pointing toward the centers of the melt pools. EBSD images also show small equiaxed grains which are indicative of the grain pool boundaries. When observing the melt pools in the optical images they appear to have no structure and are similar to the melt pools observed in the Conventional Slow samples.

The calculated energy density for the Conventional Fast samples promotes high surface roughness parameters. This is because the high velocity results in not enough energy being put into the powder particles to fully melt them. This causes the satellites to form on the surface of the sample. The surface roughness value from non-contact optical profilometry is the highest of the AM SLM samples which is 30.8 μm.

Proprietary High with the highest energy density had finer grain structure because of the above mentioned melt pool boundaries created by the build parameters which allowed for this sample to have one of the lowest calculated wear rates. Conventional Slow had one of the lowest calculated energy densities at 0.47 J/mm^2 similar to Conventional Fast however, the microstructure of the sample is different having oriented long columnar gains. This sample also has melt pool boundaries that differ from the Proprietary High samples that are randomly dispersed along the contour surface. Therefore, the differences that were observed in the microstructure impacts the wear rate causing it to be low.

The roughness values of all of the samples promote high wear rates when compared to smoother samples and most surface roughness parameters of post stress relieved AM SLM parts will also be significantly higher than the conventional counterparts. Therefore, part 2 of the tribological wear testing was performed which looked at all samples with a surface finished surface with the measured roughness values between 0.2 μm and 0.5 μm.

7.2 Wear Mechanics of Post Stress Relieved AM SLM Samples

The surface finished conventional AA2618 and AA4032 samples had a lower calculated wear rate when compared to the surface finished AM SLM samples. After the conventional AA2618 and AA4032, AM SLM Proprietary High had the next lowest calculated wear and followed closely by Conventional Slow. Proprietary Low and Conventional Fast had the highest calculated wear rates. The visual appearance of the wear scars of the Conventional Slow, Proprietary Low, and Conventional Fast AM SLM samples all had variable wear scar depth across the imaged area and they also had pile up on the sides of the wear tracks. These features could be indicative of debris generation during the wear testing with the debris infiltrating the wear tracks and causing the variability. The pile up that is observed on the sides of the wear scars could also indicate differences in other mechanical properties that were not studied in this investigation.

Since the samples were surface finished to remove surface roughness some of the melt pool geometry features were removed. The Conventional Slow and Conventional Fast samples did not have any unique features with the melt pool geometries near the surface, therefore these samples are the same as the post stress relieved versions which were described above. The Proprietary Low sample had a structured melt pool feature on the contour surface which was approximately 125 µm wide. This feature has been removed with the surface finishing technique. Therefore, the melt pool geometry looks similar to the Conventional Slow and Conventional Fast. The Proprietary High sample had large melt pools that spanned approximately 500 µm into the bulk of the sample from the contour surface. This feature has only been partially removed with the surface finishing technique. Figure 15d shows the remaining melt pool geometry which is approximately 150 µm wide.

The wear rate of the AA2618 was the lowest compared with the other samples and this material has unique properties that correlate to the observed wear resistance. AA2618 aluminum alloy is alloyed with iron and nickel that is controlled at a 1:1 ratio and these elements form the intermetallic phase of Al_9FeNi which is known to increase the resistance to plastic deformation and therefore reduce the wear rate. This controlled ratio also allows for the intermetallic phase of Al_2CuMg to form which is known to strengthen the alloy. (Balducci, 2017, Novy, 2009) These alloying elements in addition to the extrusion process and tempering procedure, T6511, that the sample has undergone which increases the hardness of the material and reduces the wear rate. Vickers hardness and Rockwell B hardness confirm the increased hardness of 25% to 50% compared to the AM SLM samples. The microstructure of the sample has equiaxed grains with iron constituents in the structure which is observed in EBSD image Figure 16e.

AA4032 material had the next lowest calculated wear rate. This material is alloyed with high amounts of silicon which makes it hyper eutectic. AA4032 is rod has been extruded which is a thermomechanical process and increases the hardness, it has also been tempered with T651 process which further increases the hardness and therefore reduces the wear rate. The EBSD images show equiaxed grains with silicon constituents in the structure which can be observed in Figure 16f. These equiaxed grains have random crystallographic orientations. Vickers hardness and Rockwell B hardness measurements confirm the increased hardness of 25% to 50% when compared to the AM SLM samples. The extrusion process and subsequent tempering improve the mechanical properties and therefore increasing the wear resistance. Therefore, the wear rate of the material is low.

Since the AM SLM samples all have similar hardness values, with Proprietary High having a slightly higher hardness, and have been polished to the same roughness this tribology testing demonstrates the importance of the build parameters and their resulting effect on the microstructure of the material and the melt pool geometries.

Proprietary High surface finished samples have the next lowest wear rate and is similar to AA4032. These samples have the structured melt pool geometries that are formed from the high energy density with the melt pools having low cooling rates and therefore producing melt pools that span approximately 500 μm and are stacking on top of each other. These melt pool boundaries have grains that are more equiaxed in shapes compared to the other AM SLM samples. The microstructure also has grains that angle towards the center of the melt pool. The unique melt pool geometries improve the wear resistance of this material. This sample also had a uniform wear scar and did not have pile up on the sides of the wear scar. This could be an indication that the hardness is increased on the sides of the melt pool boundaries allowing for better wear resistance.

A future study would be to complete nanoindentation along the melt pools to gain a better understanding of the hardness in the different areas of the melt pools, such as the boundaries versus the centers.

Conventional Slow wear rate was also comparable to the conventional AA4032 material. However, the wear scar of this sample has differences in depths across the non-contact optical profilometer image and these depth changes may be indicative of debris generation and infiltration into the wear scar. The wear scar also has pile up on the sides creating a coarse appearance. The microstructure of this material is long columnar grains that are crystalographically oriented in the <001> direction which is unique to this build parameter set and has small equiaxed grains where the melt pool boundaries are located. The melt pool geometries have no unique features and are similar to that of surface finished Proprietary Low and Conventional Fast samples. Therefore, the microstructure of the material that is unique compared to the other AM SLM samples is causing the increased wear resistance of the material.

This data suggests that with more studies understanding the effects of build parameters on microstructure, melt pools, and mechanical properties AM SLM samples may be able to be used in conventional applications that experience wear and have improved performance over conventional materials.

7.3 Conclusions

One hypothesis of this study was that the wear performance of aluminum alloys can be optimized using SLM additive manufacturing, particularly using increased energy density to achieve a fine grain structure resulting in high hardness and high wear resistance. This hypothesis was partially validated with the increase energy density samples, Proprietary Low and Proprietary High, having a finer grain structure near the melt pool boundaries over the Conventional Slow and Conventional Fast which is due to the slower cooling rates that these build parameters allow. However, the AM SLM materials did not demonstrate a higher hardness. This was investigated and determined to be caused by the stress relief temperature that was recommended by EOS to remove anisotropy from the part. As stated previously future work could include stress relieving samples at various temperatures and observing the microstructure variations, hardness variations and performing wear tests to understand the differences in the wear mechanics. However, even without the higher hardness there were two AM SLM samples that had comparable performance to the conventional AA4032 aluminum alloy which were Proprietary High and Conventional Slow. These samples both had a unique microstructure feature that increased the wear resistance, for the Proprietary High sample it was the melt pool boundaries and the for Conventional Slow it was the crystalographically oriented long columnar grains.

Another hypothesis of this investigation was that by adjusting build parameters of the AM SLM samples, the resulting component can have different resulting microstructures, porosity, and surface roughness parameters which can further modify wear resistance. Four different build parameter sets were used during this investigation. The first set of build parameters was Conventional Slow which had laser power of 80 W, velocity of 900 mm/s, and hatch spacing of 0.19 mm. These parameters had a calculated energy density of 0.47 J/mm^2 using equation 2-1. The second set of build parameters was labeled Proprietary Low. This sample had a hatch spacing of 0.19 mm and a calculated energy density that was increased from Conventional Slow. The third set of build parameters was Proprietary High which had a hatch spacing of 0.10 and a calculated energy density that was increased from Proprietary Low. The last set of build parameters was

Conventional Fast and had a laser power of 210 W, a velocity of 2360 mm/s, and hatch spacing of 0.19 mm. These parameters had a calculated energy density of 0.47 J/mm^2 which is the same as Conventional Slow.

The four build parameter sets all produced different surface roughness parameters with the Proprietary Low and Proprietary High having the lowest roughness which is because the ratio of laser power and velocity was able to fully melt the powder particles and not produce satellites which cause increases in roughness. The samples all had similar amounts of porosity so there was negligible impact from these build parameters on the porosity of the samples. However, all four samples had different microstructures and melt pool geometries which were described in detail earlier in the conclusions section.

An addition to this hypothesis is that while additive manufacturing is known to produce parts with high roughness in their as-printed state, surface finishing techniques can be used to reduce surface roughness parameters to eliminate this factor. This surface finishing technique help to eliminate the roughness factor and allowed two of the four build parameter sets, Proprietary High and Conventional Slow to produce wear rates that were similar to the conventional materials.

To summarize there is a relationship between build parameters and the resulting microstructure and melt pool geometries. Additive manufactured selective laser melted Proprietary High samples which had the highest calculated energy density had a microstructure which has grains in a random crystallographic orientation that were a combination of columnar and equiaxed at the melt pool boundaries. The melt pool geometry was structured with the pools directly on top of one another because of the slow cooling rates. This build parameter set has offered improved wear resistance compared to the other AM SLM samples. The AM SLM Conventional Slow sample also showed an improvement in wear rate compared to the Proprietary

Low and Conventional Fast. The unique feature that this samples has is long columnar grains that are oriented in the <001> direction which allows for the sample to have improved wear rate. The future studies that were proposed would help to gain a better understanding of why these build parameters were able to increase the wear resistance and perform similarly to the conventional AA4032 aluminum alloy. These studies would help to have a better understanding of the melt pool geometries and the potential hardness variations throughout the melt pool, the stress relief process and its impact on mechanical properties and wear resistance, and understanding the evolution of the microstructure around the wear scar by EBSD analysis.

Bibliography

Alicona. (2019) Retrieved January 5, 2019, from https://www.alicona.com/en/focus-variation/

Aluminum 2618-T61. (2019) Retrieved January 5, 2019, from http://www.matweb.com/search/datasheet_print.aspx?matguid=f6d0bebbfc7248838243b7fa141431ba

Aluminum 4032-T6. (2019) Retrieved January 5, 2019, from http://www.matweb.com/search/datasheetText.aspx?bassnum=MA4032T6

ASTM Standard E92, 2017, "Standard Test Methods for Vickers Hardness and Knoop Hardness of Metallic Materials," ASTM International, West Conshohocken, PA, 1952. doi: 10.1520/E0092-17

Balducci, E., Ceschini, L., Morri, A., Morri, A. (2017) EN AW-4032 T6 Piston Alloy After High-Temperature Exposure: Residual Strength and Microstructural Features. *Journal of Materials Engineering and Performance, 26,* 3802-3812. doi: 10.1007/s11665-017-2835-z

Barbieri, S. G., Giacopini, M., Mangerugo, V., Mantovani, S., (2017) A Design Strategy Based on Topology Optimization Techniques for an Additive Manufactured High Performance Engine Piston. *Procedia Manufacturing, 11,* 641-649. doi: 10.1016/j.promfg.2017.07.162

Bartolo, P. J., Lemos, A. C, Pereira, A. M., Mateus, A. J., Ramos, C., Santos, C., Oliveira, D., Pinto, E. (2013) *High Value Manufacturing: Advanced Research in Vitual and Rapid Prototyping.*

Bourell, D., Kruth, J. P., Leu, M., Gideon, L., Rosen, D., Beese, A., Clare, A. (2017) Materials for Additive Manufacturing. *CIRP Annals – Manufacturing Technology*, *66,* 659-681. doi: 10.1016/j.cirp.2017.05.009

Elgallad, E. M., Shen, P., Zhang, Z., Chen, X. G. (2014) Effects of Heat Treatment on the Microstructure and Mechanical Properties of AA2618 DC Cast Alloy. *Materials and Design, 61,* 133-140. doi: 10.1016/j.matdes.2014.04.045

EOS Aluminum AlSi10Mg Material Data Sheet. (2014, May). Retrieved November 1, 2018, from https://gpiprototype.com/pdf/EOS_Aluminum_AlSi10Mg_en.pdf

Ethanol, 200 Proof. (2019) Retrieved March 12, 2019, from http://www.matweb.com/search/datasheet.aspx?matguid=ce6c484c48a44e3c9bb23ea3185741d5&ckck=1

Fildes, J. M., Kilaparti, R., Schlepp, E. (2018) Quantifying Abrasive and Adhesive Wear of Coatings with a Ball on Three Disk Configuration. *Wear,* 1-10.

Han, Q., Jiao, Y. (2019) Effect of Heat Treatment and Laser Surface Remelting on AlSi10Mg Alloy Fabricated by Selective Laser Melting. *The International Journal of Advanced Manufacturing Technology,* 1-10. doi: 10.1007/s00170-018-03272-y

Hanzl, P., Zetek, M., Baksa, T., Kroupa, T. (2015) The Influence of Processing Parameters on the Mechanical Properties of SLM Parts. *Procedia Engineering, 100,* 1405-1413. doi: 10.1016/j.proeng.2015.01.510

Herzog, D., Seyda, V., Wycisk, E., Emmelmann, C. (2016) Additive Manufacturing of Metals. *Acta Materialia, 117,* 371-392. doi: 10.1016/j.actamat.2016.07.019

Iturrioz, A., Gil, E., Petite, M. M., Garciandia, F., Mancisidor, A. M., Sebastian, M. S. (2018) Selective Laser Melting of AlSi10Mg Alloy: Influence of Heat Treatment Condition on Mechanical Properties and Microstructure. *Welding in the World, 62,* 885-892. doi: 10.1007/s40194-018-0592-8

Kang, N., Coddet, P., Liao, H., Baur, T., Coddet, C. (2016) Wear Behavior and Microstructure of Hypereutectic Al-Si Alloys Prepared by Selective Laser Melting. *Applied Surface Science, 378,* 142-149. doi: 10.1016/j.apsusc.2016.03.221

Kauzlarich, J. J., Williams, J. A. (2001) Archard Wear and Component Geometry. *Proceedings of the Institution of Mechanical Engineered, 215,* 387-403.

Krishnan, M., Atzeni, E., Canali, R., Calignano, F., Manfredi, D., Ambrosio, E. P., Iuliano, L. (2014) On the Effect of Process Parameters on Properties of AlSi10Mg Parts Produced by DMLS. *Rapid Prototyping Journal, 20,* 449-458. doi: 10.1108/RPJ-03-2013-0028

Kurzynowski, T., Chlebus, E., Kuznicka, B., Reiner, J. (2012) Parameters in Selective Laser Melting for Processing Metallic Powders. *High Power Laser Materials Processing Conference, 8239,* 1-8. doi: 10.1117/12.907292

Li, W., Li, S., Liu, J., Zhang, A., Zhou, Y., Wei, Q., Yan, C., Shi, Y. (2016) Effect of Heat Treatment on AlSi10Mg Alloy Fabricated by Selective Laser Melting: Microstructure Evolution, Mechanical Properties and Fracture Mechanism. *Materials Science and Engineering A, 663,* 116-125. doi: 10.1016/j.mesa.2016.03.088

Maamoun, A. H., Xue, Y. F., Elbestawi, M. A., Veldhuis, S. C., (2018) Effect of Selective Laser Melting Process Parameters on the Quality of Al Alloy Parts: Powder Characterization, Density, Surface Roughness, and Dimensional Accuracy. *Materials, 11, 2343,* 1-21. doi:10.3390/ma11122343

Mbuya, T. O., Sinclair, I., Moffat, A. J., Reed, P. A. S. (2012) Micromechanisms of Fatigue Crack Growth in Cast Aluminum Piston Alloys. *International Journal of Fatigue, 42,* 227-237. doi: 10.1016/j.ifatigue.2011.10.015

Novy, F., Janecek, M., Kral, R. (2009) Microstructure Changes in a 2618 Aluminum Alloy During Ageing and Creep. *Journal of Alloys and Compounds, 487,* 146-151. doi: 10.1016/j.jallcom.2009.08.014

Piston and Piston Rings. (1996, October 11). Retrieved November 11, 2018, from https://courses.washington.edu/engr100/Section_Wei/engine/UofWindsorManual/Piston%20and%20Piston%20Rings.htm

Scanning Electron Microscopy (SEM). (2017). Retrieved November 1, 2018, from https://serc.carleton.edu/research_education/geochemsheets/techniques/SEM.html

Schikorra, M., Donati, L., Tomesani, L., Tekkaya, A. E. (2007) Microstructure Analysis of Aluminum Extrusion: Grain Size Distribution in AA6060, AA6082, and AA7075 Alloys. *Journal of Mechanical Science and Technology, 21,* 1445-1451.

Trevisan, F., Calignano, F., Lorusso, M., Pakkanen, J., Aversa, A., Ambrosio, E. P., Lombardi, M., Fino, P., Manfredi, D. (2017) Review on the Selective Laser Melting (SLM) of the AlSi10Mg Alloy: Process, Microstructure, and Mechanical Properties. *Materials, 76,* 1-23. doi: 10.3390/ma10010076

Valigi, M. C., Logozzo, S., Affatato, S. (2017) New Challenges in Tribology: Wear Assessment Using 3D Optical Scanners. *Materials, 10, 548*, 1-13. doi: 10.3390/ma10050548

Water, H_20. (2019) Retrieved March 12, 2019, from http://www.matweb.com/search/DataSheet.aspx?MatGUID=64a0e072a9ec430e92ed984c7131b690

White, J., Read, N., Ward, R. M., Mellor, R., Attallah, M. M. (2014) Prediction of Melt Pool Profiles for Selective Laser Melting of AlSi10Mg Alloy. *ResearchGate.*

Zescope Optical Profiler Combines 3D Surface Metrology with Ease of Use. (2009, October 19). Retrieved January 5, 2019, from https://microscopy-news.com/archive/zescope-optical-profiler-combines-3d-surface-metrology-with-ease-of-use/

Zhu, Y., Zou, J., Yang, H. (2018) Wear Performance of Metal Parts Fabricated by Selective Laser Melting: A Literature Review. *Journal of Zhejiang University – Science A, 19,* 95-110. doi: 10.1631/jzus.A1700328

Zygula, K., Nosek, B., Pasiowiec, H., Szysiak, N. (2018) Mechanical Properties and Microstructure of AlSi10Mg Alloy Obtained by Casting and SLM Technique. *World Scientific News, 104,* 462-472.